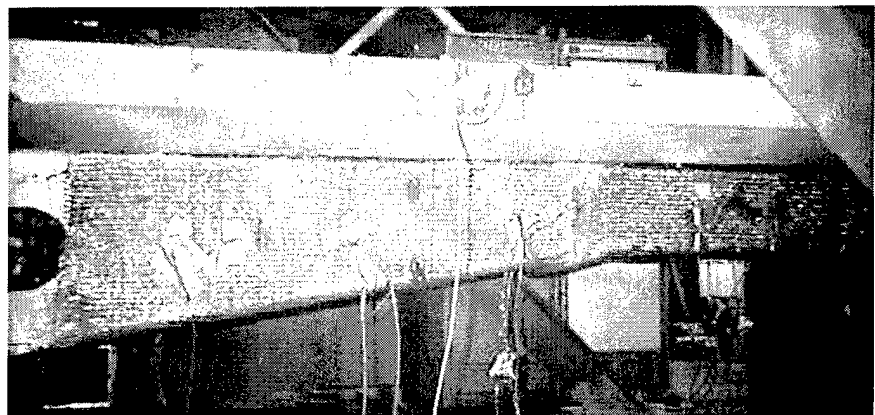# Shear Strengthening of Reinforced Concrete Beams Using Fiber-Reinforced Polymer Wraps

Pamalee A. Brady and Orange S. Marshall

Studies have shown that fiber-reinforced polymer (FRP) wraps can improve the capacity of rectangular beam sections. This technology has potential application to highway bridges that may have less shear capacity than flexural capacity or require added load capacity to handle current traffic demands. Compared with steel repair materials FRP offers several benefits, such as corrosion resistance and field-workability. Several studies have investigated the use of externally bonded FRP sheets to improve strength and stiffness of reinforced concrete (R/C) beams, but most have addressed flexural strength, not shear.

The objective of the current study was to test the effectiveness of FRP wraps in repairing full-scale prestressed high-strength concrete joists fabricated with insufficient shear reinforcement. Four prestressed high-strength concrete tee-beams (joists) with integral web openings were tested. Two of the joists were repaired or upgraded with FRP wraps to improve shear performance and two were used as control specimens. Performance criteria were specified, and standard structural engineering practice for shear design was employed to determine wrap thickness. The results of the tests indicate that significant increases in the shear strength of R/C beams with insufficient shear capacity can be achieved by proper application of FRP wraps.

19990203 077

USER EVALUATION OF REPORT

REFERENCE: USACERL Special Report 99/01, *Shear Strengthening of Reinforced Concrete Beams Using Fiber-Reinforced Polymer Wraps*

Please take a few minutes to answer the questions below, tear out this sheet, and return it to USACERL. As user of this report, your customer comments will provide USACERL with information essential for improving future reports.

1. Does this report satisfy a need? (Comment on purpose, related project, or other area of interest for which report will be used.)

_____

_____

_____

2. How, specifically, is the report being used? (Information source, design data or procedure, management procedure, source of ideas, etc.)

_____

_____

3. Has the information in this report led to any quantitative savings as far as manhours/contract dollars saved, operating costs avoided, efficiencies achieved, etc.? If so, please elaborate.

_____

_____

4. What is your evaluation of this report in the following areas?

a. Presentation: _____

b. Completeness: _____

c. Easy to Understand: _____

d. Easy to Implement: _____

e. Adequate Reference Material: _____

f. Relates to Area of Interest: _____

g. Did the report meet your expectations? _____

h. Does the report raise unanswered questions? _____

i. General Comments. (Indicate what you think should be changed to make this report and future reports of this type more responsive to your needs, more usable, improve readability, etc.)

_____

_____

_____

_____

_____

_____

5. If you would like to be contacted by the personnel who prepared this report to raise specific questions or discuss the topic, please fill in the following information.

Name: _____

Telephone Number: _____

Organization Address: _____

_____

_____

6. Please mail the completed form to:

Department of the Army
CONSTRUCTION ENGINEERING RESEARCH LABORATORIES
ATTN: CECER-TR-I
P.O. Box 9005
Champaign, IL 61826-9005

REPORT DOCUMENTATION PAGE	*Form Approved* *OMB No. 0704-0188*

Public reporting burden for this collection of information is estimated to average 1 hour per response, including the time for reviewing instructions, searching existing data sources, gathering and maintaining the data needed, and completing and reviewing the collection of information. Send comments regarding this burden estimate or any other aspect of this collection of information, including suggestions for reducing this burden, to Washington Headquarters Services, Directorate for information Operations and Reports, 1215 Jefferson Davis Highway, Suite 1204, Arlington, VA 22202-4302, and to the Office of Management and Budget, Paperwork Reduction Project (0704-0188), Washington, DC 20503.

1. AGENCY USE ONLY *(Leave Blank)*	2. REPORT DATE October 1998	3. REPORT TYPE AND DATES COVERED Final	
4. TITLE AND SUBTITLE Shear Strengthening of Reinforced Concrete Beams Using Fiber-Reinforced Polymer Wraps			5. FUNDING NUMBERS CPAR LW4
6. AUTHOR(S) Pamalee A. Brady and Orange S. Marshall			
7. PERFORMING ORGANIZATION NAME(S) AND ADDRESS(ES) U.S. Army Construction Engineering Research Laboratories (USACERL) P.O. Box 9005 Champaign, IL 61826-9005			8. PERFORMING ORGANIZATION REPORT NUMBER SR 99/01
9. SPONSORING / MONITORING AGENCY NAME(S) AND ADDRESS(ES) Headquarters, U.S. Army Corps of Engineers ATTN: CEMP-CE 20 Massachusetts Ave. NW Washington, DC 20314-1000			10. SPONSORING / MONITORING AGENCY REPORT NUMBER

11. SUPPLEMENTARY NOTES
Copies are available from the National Technical Information Service, 5285 Port Royal Road, Springfield, VA 22161.

12a. DISTRIBUTION / AVAILABILITY STATEMENT Approved for public release; distribution is unlimited.	12b. DISTRIBUTION CODE

13. ABSTRACT (Maximum 200 words)

Studies have shown that fiber-reinforced polymer (FRP) wraps can improve the capacity of rectangular beam sections. This technology has potential application to highway bridges that may have less shear capacity than flexural capacity or require added load capacity to handle current traffic demands. Compared with steel repair materials FRP offers several benefits, such as corrosion resistance and field-workability. Several studies have investigated the use of externally bonded FRP sheets to improve strength and stiffness of reinforced concrete (R/C) beams, but most have addressed flexural strength, not shear.

The objective of the current study was to test the effectiveness of FRP wraps in repairing full-scale prestressed high-strength concrete joists fabricated with insufficient shear reinforcement. Four prestressed high-strength concrete tee-beams (joists) with integral web openings were tested. Two of the joists were repaired or upgraded with FRP wraps to improve shear performance and two were used as control specimens. Performance criteria were specified, and standard structural engineering practice for shear design was employed to determine wrap thickness. The results of the tests indicate that significant increases in the shear strength of R/C beams with insufficient shear capacity can be achieved by proper application of FRP wraps.

14. SUBJECT TERMS concrete structural engineering fiber-reinforced polymer (FRP) composite materials			15. NUMBER OF PAGES 78
			16. PRICE CODE
17. SECURITY CLASSIFICATION OF REPORT Unclassified	18. SECURITY CLASSIFICATION OF THIS PAGE Unclassified	19. SECURITY CLASSIFICATION OF ABSTRACT Unclassified	20. LIMITATION OF ABSTRACT SAR

NSN 7540-01-280-5500

Standard Form 298 (Rev. 2-89)
Prescribed by ANSI Std 239-18
298-102

Foreword

Contents

List of Figures and Tables

Figures

Tables

1 Introduction

Background

Previous studies of rectangular beams have shown that fiber-reinforced polymer (FRP) wraps of the full cross section improve the capacity of the section. The challenge of applying an FRP wrap to a beam with slab and the benefits of such an upgrade have not been assessed. This technology has potential application to highway bridges constructed in accordance with American Concrete Institute (ACI) codes of the 1950s and 1960s where these bridges may have less shear capacity than flexural capacity, or where added load capacity is required. A proven repair method for this reinforced concrete (R/C) application may provide a cost-effective solution for military installations and Corps of Engineers civil works facilities, as well as civilian departments of transportation.

Shear repair of reinforced concrete beams using externally bonded materials is not a new concept. For many years, sheets of steel were applied to the tensile face of damaged beams. The steel was effective in increasing both the shear and flexural capacities of the member, but there have been two major disadvantages to this method. First, bonding the steel to the beam is quite difficult in the field due to its bulk. Second, the new plate is susceptible to corrosion, which can cause loss of the adhesive bond.

An innovative method of beam shear repair involves the use of FRP externally bonded to the faces of the member where shear capacity is deficient. Several schemes are available: FRP plates bonded to the sides, strips of FRP material bonded to the sides, or a jacket (wrap) placed along the shear span. FRP addresses the traditional material weaknesses of steel discussed above: it is not susceptible to corrosion and is relatively conducive to field prepping and hand lay-up. There have been several studies investigating the use of externally bonded FRP sheets to improve strength and stiffness of R/C beams, but most of these have dealt with improving beam flexural strength. Only a few studies have specifically addressed shear.

Al-Sulaimani et al. (1994) tested simply supported R/C beams with fiberglass in all three configurations (plates, strips, and wrap) under four-point loading. The specimens were 6 in. x 6 in. in cross section and 49.2 in. in length. Compression

and tension reinforcement as well as web stirrups were present. These beams were pre-damaged before retrofit and were designed to fail in shear (the stirrups served mostly to confine the flexural reinforcement). The researchers determined that fiberglass plates and strips bonded to the sides of the beams produced a modest (25-30%) increase in shear capacity. This repair technique, however, did not provide enough of an improvement to prevent a shear mode of failure. Also, the fiberglass plates and strips peeled off. Beams fitted with a fiberglass wrap, however, nearly doubled the beams' shear capacity, and this increase was sufficient to produce a flexural (i.e., not shear) mode of failure.

Chajes et al. (May 1995) investigated R/C beams with aramid, glass, and graphite wraps loaded in four-point bending. These specimens were structural tees in cross section having a 7.5 in. depth, 5.5 in. wide flange, 2.5 in. thick web, and 48 in. length. These beams were completely lacking in shear reinforcement but contained enough flexural reinforcement (only tension steel) such that a shear failure would occur. While all beams experienced an increase in ultimate capacity they still failed in shear. The glass and graphite wraps were torn along the diagonal crack. The aramid wrap allowed the failed beams to carry some load, however. It is important to note that the purpose of this experimentation was not to force flexural failure, but to determine the effectiveness of the system to increase shear capacity in specimens that were designed to fail in shear. Therefore, the FRP wrap was shown to be effective for shear repair. Chajes et al. published another paper (1995) where the beams were designed to fail in flexure. The only shear reinforcement would be provided by the FRP wrap. In that experiment the beams developed sufficient shear capacity and failed in flexure, as designed.

Based on the results of the studies cited above, it is known that composite wraps are potentially very effective in shear rehabilitation of reinforced concrete. Both research groups concluded that there was a need for full-scale testing of this technology. In 1997 the U.S. Army Construction Engineering Research Laboratories (CERL) conducted such testing as part of a broader investigation of concrete repair technologies funded and executed under the Army Corps of Engineers Construction Productivity Advancement Research (CPAR) program. The results of this testing were published as an appendix to the final CPAR report (Marshall et al., February 1998), but they are presented here on their own to reach engineers and materials scientists interested in the specific problem of composite-based repair techniques to improve the shear performance of existing R/C structures.

Objective

The objective of this study was to test the effectiveness of FRP-based repair techniques on full-scale prestressed high-strength concrete joists fabricated with insufficient shear reinforcement.

Approach

Four prestressed high-strength concrete tee-beams (joists) with integral web openings were tested. Two of the joists were used as control specimens. One control joist had insufficient shear reinforcement and one was properly reinforced, designated HJ-6 and HJ-7, respectively. The other two joists were repaired (HJ-4) or upgraded (HJ-3) with FRP to improve their shear performance. Performance criteria were specified for the two joists to be repaired. HJ-3 and HJ-4 were wrapped on three sides, along the outer 8 ft of each end, with an FRP composite system called TYFO S Fibrwrap™. Standard structural engineering practice for shear designs was used to determine the wrap thickness. Calculations were based on controlling shear crack widths to maintain aggregate interlock and proper shear transfer through the concrete.

Technical details about test specimen fabrication, repair material properties and specifications, shear reinforcement techniques, and testing procedures are presented in Chapter 3.

Mode of Technology Transfer

A version of the material presented here was included as an appendix to CERL Technical Report TR 98/47 (Marshall et al., February 1998); that report presented the current topic within a much broader concrete repair context.

A number of FRP composite systems are already on the market for the repair, strengthening, or seismic upgrade of unreinforced or lightly reinforced masonry structures, and new products are regularly becoming available. The FRP/URM Project Team of the Composites Institute Market Development Alliance (CI/MDA) is establishing a database of contacts for companies that market these types of structural enhancement systems. For further information contact Manager, Market Development, Composites Institute, 600 Mamaroneck Ave., Harrison, NY 10528-1632 (914-381-1253, x256 voice; 914-381-1253 fax).

Units of Weight and Measure

U.S. standard units of measure are used throughout this report. A table of conversion factors for Standard International (SI) units is provided below.

SI conversion factors		
1 in.	=	2.54 cm
1 ft	=	0.305 m
1 yd	=	0.9144 m
1 sq in.	=	6.452 cm^2
1 sq ft	=	0.093 m^2
1 sq yd	=	0.836 m^2
1 cu in.	=	16.39 cm^3
1 cu ft	=	0.028 m^3
1 cu yd	=	0.764 m^3
1 gal	=	3.78 L
1 lb	=	0.453 kg
1 kip	=	453 kg
1 psi	=	6.89 kPa
°F	=	(°C x 1.8) + 32

2 Fiber-Reinforced Composites

A composite is a combination of two or more materials (reinforcing elements, fillers, and matrix binder) with different form or composition which, when combined into a material system, exhibit properties which are a combination of its individual components. The system constituents retain their distinct identities, meaning they do not dissolve or merge completely into each other, but act in concert to provide an overall function. The matrix can be a ceramic, metal, or polymer. Fillers may be mineral or metallic powders. Reinforcing can be particles, fibers, rods, or bars. For example, reinforced concrete is a composite consisting of steel reinforcement, sand and gravel fillers, and a portland cement matrix.

Fiber-reinforced composites or fiber-reinforced polymers (FRP) consist primarily of a typical reinforcement of glass, carbon or aramid fibers, and a polymer matrix. Fillers to modify the physical, mechanical, thermal, electrical, and other properties or to lower the cost or density, may or may not be included. The polymer matrix may be a thermoplastic, a thermoset, or an elastomer. A thermoplastic polymer, polyethylene, polyvinyl chloride, or polystyrene for example, is one which becomes pliable or plastic when heated and then becomes hard again when cooled. A thermoset polymer changes into a crosslinked, substantially infusible material when cured by heat or chemical reaction. Epoxy, polyester, and polyurethane are examples of thermosets. An elastomer is a rubber-like polymer which recovers its original shape and size after removal of a deforming force.

The key component of an FRP is the fibrous reinforcement; it is the primary load bearing component. The matrix serves as the mechanism by which loads are transferred within the member from one fiber to another. Each type of fiber has certain advantages and disadvantages; reinforcement is selected on the basis of its physical, mechanical, and thermal properties.

Modern glass fibers were first developed in the 1930s for military purposes. Soon after, its primary commercial use was for the reinforcement of plastics. E-glass is the standard because of its electrical and mechanical properties. This fiber has a tensile strength nearly double that of steel and has modified versions that resist strong acids. An interesting characteristic of glass fibers is that they are elastic — elongating until failure without yielding. After the load is released the fiber returns to its original length.

Carbon fibers are the most widely used variety of reinforcement having a very wide range of physical properties. Their strength can vary from that of steel to about four times that. What separates carbon fiber reinforced polymer (CFRP) from the rest is its low weight. Its performance based on stiffness to density is very high. It also has very good fatigue and damping characteristics. Manufactured carbon fibers can vary from the weakest of all fibers to among the strongest. Likewise, their price also varies from inexpensive for the weaker fibers to expensive for the strongest fibers. The most commonly produced versions of CFRP are the intermediate strength fibers. They have tensile strengths stronger than glass and somewhat weaker than aramids.

Like carbon, aramid fibers are lightweight, have high tensile strengths, and good damping and wear resistance. They also have excellent fiber toughness. A popular version of the aramid fiber is marketed under the trademark Kevlar. However, its drawbacks are low resistance to acid attack and high cost.

As the manufacture of FRP composites improve and their mechanical properties are better understood, they are being used in a wider variety of applications. Because of the ultra-conservative nature of the civil engineering community and the relatively short history of FRP composites use, fiber-reinforced composites are just beginning to be considered as a civil engineering material alternative to steel and reinforced concrete. Although many factors, including material form, will significantly influence any design, some general differences between metals and composites may make the latter appear to be the more attractive choice. Differences between composites and metals are as follows:

- Unidirectional aramid and carbon fiber reinforced epoxies provide a specific tensile strength (ratio of material strength to density) that is approximately four to six times greater than that of steel or aluminum

- Unidirectional carbon fiber reinforced epoxies provide a specific modulus (ratio of material stiffness to density) that is approximately 3½ to 5 times greater than that of steel or aluminum. Aramid falls between carbon and glass fiber reinforced epoxies

- Comparing efficiently designed structural elements, the fatigue endurance limit for aramid and carbon fiber reinforced epoxies may approach 60% of the ultimate tensile strength. For aluminum and steel, this value is considerably lower

- Because of the properties listed above, aramid, carbon, and hybrid fiber reinforced plastics can provide structures that are 25 to 45% lighter than aluminum structures designed to the same functional requirements. Impact energy values for aramid-epoxy composites are significantly higher than those for carbon fibers and aerospace aluminum alloys

- Fiber-reinforced polymers can be designed with excellent structural damping features to provide lower vibration transmission than metals
- Fibrous composites are more versatile than metals and can be tailored to meet performance needs and complex design requirements. Design requirements sometimes cannot be satisfied by metal alloys within the critical weight limitations
- The properties mentioned above can be balanced with cost by hybridization (mixing different fibers in a given composite to attain an optimum combination of properties)
- Corrosion and other attributes of fibrous composites will contribute to reduced lifecycle cost
- Composite parts can eliminate joints/fasteners, providing part simplification and integrated design

FRP composites consist primarily of fiber reinforcement and a polymer. Fibers that are typically used for civil and structural engineering applications are E-glass, carbon, and aramid; polymers are either polyester, vinyl ester, or epoxy. A major reason these polymers are used is because they cure by chemical reaction at ambient temperature. FRP composites may take several forms. The fibers can be in a woven or stitched fabric, or unidirectional sheet, tow or yarn. The composite may be a prepreg (fabric with uncured polymer infusion at the factory), preform (extruded, cast, or shaped at the factory), laminate plate, rod/cable, or a hybrid of these. Various methods exist for applying composites to a structural member. They include hand lay-up, filament winding, vacuum resin transfer molding, and any compaction process. When preforms or laminate plates are used for repair or upgrade, matrix binders or adhesives made of polyester, vinyl ester, epoxy, or polyurethane are used to bond them to the structural members. Depending upon the composite specifications, additives, fillers, or coatings may also be incorporated in the composite to provide UV and/or fire resistance and special moisture or chemical resistance.

3 Experimental Program

Test Specimens

The hybrid joist design used in the experiments is intended to combine the benefits of prestressed concrete double tees and open-web steel joists but overcome their shortcomings. The hybrid joist was envisioned for use in office construction. A length of 32 ft and a tributary width of 8 ft were chosen for the initial design. Loads of 50 psf office live load and 20 psf superimposed dead load were assumed. All loads were assumed to be uniformly applied along the joist length. This resulted in a superimposed total uniform service load of 70 psf and an ultimate load of 113 psf.

The overall configuration of the joist is shown in Figure 1.[*] The joist webs had a constant thickness of 6 in. Joist web ends were 10 in. deep; the depth of all other joist web elements was 6 in. Overall depth of the web was 24 in. Three openings were located along the joist length. Prestressing tendons were located in the top and bottom chords of the web. The prestressing tendon profile is shown in Figure 2. Six tendons were used, two straight and four draped. Figure 3 summarizes the web reinforcement of each of the beams. The cast-in-place concrete flanges of HJ-3 and HJ-4 had a thickness of 4 in. and width of 6 ft. The flanges of joists HJ-6 and HJ-7 were 4 ft wide. The slab was reinforced with welded wire fabric (WWF), 4 X 4-W4.0 X W4.0, placed at a height of 2 in. Detailed descriptions of each joist design are provided in Saleh, Brady, Einea, Tadros, and Decker (1997).

Four prestressed high-strength concrete tee-beams with integral web openings were tested. Two joists were used as control specimens. One control joist had insufficient shear reinforcement; one joist was properly reinforced, designated HJ-6 and HJ-7 respectively. The other two joists were repaired, HJ-4, or up-

---

[*] All figures and tables are presented at the end of this report.

graded, HJ-3, with FRP to improve their shear performance. Joist designations are shown in Table 1.

Performance criteria were specified for the two joists to be repaired. It was required that their shear capacity be increased 15 kips over a length 3 ft-10 in. from each end and 10 kips over the following 4 ft. The two repaired beams were wrapped on three sides with Fyfe's TYFO S Fibrwrap™ along the outer 8 ft of each end of HJ-3 and HJ-4, Figure 4. The FRP repair design was based on the following material properties:

f_{sj} = 12 ksi (conservative estimate of allowable jacket stress)

f_{uj} = 65 ksi (ultimate jacket stress, minimum)

E_j = 3250 ksi (modulus of elasticity of jacket)

ε_{aj} = 0.004 (allowable jacket strain)

ε_{uj} = 0.02 (ultimate jacket strain)

u_{aj} = 400 psi (allowable bond stress)

t_j = 0.051 in. (jacket thickness per layer)

Standard structural engineering practice for shear designs was used to determine the jacket thickness. Calculations were based on controlling shear crack widths to maintain aggregate interlock and proper shear transfer through the concrete. The allowable jacket strain, εaj = 0.004, represents 20% of the ultimate composite strain. The calculations resulted in the requirement for two layers of SEH-51, with the main fiber strength vertical, over the extreme 4 ft. The next 4 ft required only one layer per the calculations, however, the Fyfe Co. recommended the use of a minimum of two layers (Gee 1996).

No additional anchorage system was used due to the potential interference with the prestressing tendons of the existing joist.

Materials

1. Concrete. The concrete mix used in the hybrid joist specimen webs was a high-performance concrete (HPC). It provided special performance requirements including ease of placement and consolidation without compromising strength, superior long-term mechanical properties, early high strength, volume stability,

and long life in severe environments. The HPC concrete strength used was designed to have a strength of 12,000 psi at 28 days. Figure 5 shows the time versus strength curves for the concrete used in the webs. Ready-mixed concrete was used in the slabs of all specimens. The mix was specified to be 5,000 psi and consisted of Type I cement with a maximum aggregate size of 1.0 in. limestone. The mix corresponded to dry weight proportions of 1.0:3.0:2.6 (cement : fine aggregate : coarse aggregate). On the day of testing all cylinders were also tested. Compression tests were conducted in accordance with ANSI/ASTM C39-86.

2. Steel. The tendons used were manufactured by the American Spring Wire Corporation (26300 Miles Rd., Cleveland, OH 44146). These tendons were 1/2 in. diameter, 270 ksi, low relaxation. The stress-strain curve for these tendons is shown in Figure 6. The shear reinforcement in the webs consisted of bar reinforcement, Grade 60. A welded wire fabric mesh, Grade 75, was used as reinforcement for the cast-in-place slab.

3. FRP. The FRP was specified as TYFO™ S Fibrwrap System and manufactured by Fyfe Co. L.L.C. of San Diego, CA. The TYFO™ S epoxy is a two-component, solvent-free, moisture insensitive epoxy matrix material. It is a high elongation material which gives optimum properties as a matrix for the TYFO™ fiber system. The epoxy has no offensive odor and maintains its properties up to 140 °F. Table 2 lists the epoxy properties. The TYFO™ fiber system is a plain weave, predominately warp unidirectional fabric comprised of a warp (0 degree orientation) of E-glass roving and a weft (90 degree orientation) of aramid, E-glass, and Thermoplastic Adhesive. The ratio of warp fiber to weft fiber is 17.5 to 1 by weight. Table 3 lists the yarn properties and Table 4 the fabric properties. Two layers of the TYFO™ S Fibrwrap System were used. Table 5 lists the composite laminate specifications and Table 6 the composite properties. The system has been tested and develops an allowable shear stress of greater than 350 psi without anchors.

Fabrication

The webs of the joists were prestressed and cast horizontally, i.e., on their sides as shown in Figure 7. Hold-down devices were used at the draping points to position the tendons and resist the prestressing forces. The concrete mix was placed in the forms and vibrated to ensure consolidation of the concrete. The specimens were covered with wet burlap that was kept moist for the first 3 days. The specimens cured at room temperature for 7 days. Cylinders measuring 4 in. diameter by 8 in. tall were cast and cured with the joists under the same conditions. The concrete strength was monitored by compression testing of cylinders to assess when the required release strength was achieved. When the strength

reached 7000 psi the tendons were released by alternately torch cutting a tendon on each face at the joist ends. Casting and release dates for each specimen are shown in Table 7. The webs were then turned vertically and stored in the lab. The webs were then positioned vertically upright and level. The slab forms were then constructed around them. After concrete placement, the forms and test cylinders were covered with wet burlap followed by plastic sheets. The burlap was maintained moist for 4 days following casting. After 7 days the forms were stripped. Figure 8 shows the final shape of the joists.

Prior to application of the composite overlay the joist surfaces were prepared. This involved removing the paint on the outer 8 ft of the webs, rounding the corners at the bottom of the beam web to a minimum radius of 1.5 in., and removing trowel marks and smoothing out rough areas using an electric grinder. Once completed, creases in the web left by the concrete form lining were filled with a rapid strength repair mortar. After the mortar was cured, the surface of the beams was again ground and then cleaned using methyl ethyl ketone to remove any excess dust. Cracks in the concrete of HJ-4 created during pre-loading were ignored since they were less than 1/16 in. wide. The two part epoxy TYFO™ S Tack Coat was mixed and troweled onto the surface of the beams where the repair/upgrade was to be applied.

While the tack coat began setting up, the reinforcing fabric was cut to the proper length using scissors and infused with the TYFO™ S two part epoxy. This was done by laying the fabric out flat and evenly spreading the resin on the fabric by hand to saturate the fabric. The fabric was then laid up around the end of the joist from just beneath the slab, around the web and up to the slab/web intersection again, Figure 9. The material was placed vertically (main fibers vertical) in bands of 52 in. (1.2m) on the sides of the joist. Adjacent bands were placed with a 4 in. butt splice. In regions of taper, the bands were applied as four pieces, two per side ensuring that main fibers remained vertical on joist faces. The material was carried under the joist and the excess cut off.

Because of lack of Cab-O-Sil™ in the tack coat, the system applicators had great difficulty getting the FRP system to adhere properly to the concrete prior to curing. The cure time was also slow because of high humidity. Upon cure it was noted that the FRP had slipped down on both HJ-3 and HJ-4. A gap, uncovered by FRP, existed beneath the bottom of the slab on the web. In most locations the gap was not significant; however, on the north end of HJ-3 the gap was observed to be 1.25 in., Figure 10. After curing, voids between the composite and the joist were filled with epoxy, Figure 11.

Instrumentation and Data Recording

Test specimens HJ-3, HJ-4, HJ-6, and HJ-7 were instrumented with displacement potentiometers, strain gages, and linear variable displacement transducers. Tables 8 and 9 summarize the instrumentation plans for HJ-3 and HJ-4. Figure 13 shows the layout of internal strain gages for HJ-3 and HJ-4. Internal strain gages were located so as to measure strains in both prestressing tendons and reinforcement. Once the composite was cured, strain gages were placed on the external surface at the locations of the most dramatic shear cracks, other previous shear failure areas, and at the FRP lap joints to monitor strain in the composite. Gages were symmetrically placed at each end of the joists. Figure 13 shows the location of these gages for HJ-3 and Figure 14 shows the gage locations for HJ-4. LVDT locations were the same for all joists (Figure 15). Displacements were measured by potentiometers at the center of the joist, beneath one web post and a distance 25% of the span length from a support along the inclined portion of the joist, Figure 16. All recorded potentiometer displacements were absolute, measured with respect to the laboratory floor. Displacement measurements were also taken manually on the west and east faces of the slab at each joist end, and along the east slab face at the center and beneath each actuator.

Figure 17 is a functional block diagram of the instrumentation, data acquisition, and test control systems used at CERL. All of the transducer output signals were connected to a Hewlett Packard[*] Model 3052A data logging system. The system was controlled by computer through an instrument controller interface bus. The record channels were scanned at a predetermined sampling rate, and the data were recorded in ASCII text files on the computer.

The loading system consisted of two CGS/Lawerence Model 307-50 electro-hydraulic actuators (controlled by closed-loop servo controllers) and a function generator. The actuators were operated in a displacement-control mode. In this mode, the function generator supplies a slowly changing command signal to the controllers. The controllers send a drive signal to each of the actuators, which causes the actuators to move until the displacement measured by LVDTs located inside each actuator is equal to the command signal. The actuators also include load transducers that measure the applied load.

---

[*] Hewlett Packard Co., 5301 Stevens Creek Blvd., Santa Clara, CA 95052-8059.

Test Procedure

The test setup on the CERL Structural Load Floor is shown in Figure 18. Each specimen was tested as a simply supported beam under two symmetrical point loads with a clear span of m (31 ft) and a shear span of m (11 ft - 3 in.). Vertical loads were applied by 50-kip hydraulic actuators suspended from a load frame. The actuators were centered directly over the web posts of the specimens. In testing at CERL the stroke of each actuator was calibrated to zero after making contact with the specimen; a small pre-load was associated with this positioning. Specimens were loaded at a constant rate to a specified stroke limit. The actuators were maintained at this stroke while the joist was inspected for cracks; these were marked. Measured readings of deflections were taken at selected locations and the deflection data were checked. Stroke was then further applied to the specimen until the stroke limit of the actuators was reached. The full stroke (i.e., full load) was then removed from the specimen. Steel plates were added between the actuator and the beam. The actuators were then moved into contact with the specimen again; this was associated with a small pre-load. The test was continued in the same manner until the specimen failed. Data were recorded during loading and unloading cycles.

Of the two repaired specimens, HJ-4 was damaged to a predetermined level defined subsequent to testing the control beams, which were unrepaired. The beam was then unloaded and repaired. HJ-3 was not loaded prior to upgrading it with FRP. After repair, the beams were loaded at a constant rate of 0.2 in./min. in increments of 1 in. At each displacement increment, measured readings of deflections were taken at selected locations and deflection data were checked. Loading of HJ-4 continued until the bottom of the joist was ¼ in. from the load floor. The joist was then unloaded. HJ-3 was loaded in the same manner as HJ-4. The joist was tested to failure.

Experimental Results

The measured load and deflection, strains in concrete, steel rebar and FRP, and crack development and failure of each specimen are discussed. Results of the two repaired beams are compared with two control beams.

Load and Deflection

Table 11 summarizes principal test results, including cracking load, location of first crack, failure load, equivalent uniform superimposed (SI) load at failure for the test configuration, and type of failure. All load values in the table represent

the sum of the two actuator loads. The experimental cracking load was determined at the time the first crack was observed. Joist HJ-4 was loaded to a peak of 55.2 kips. After the FRP repair, HJ-4 was reloaded to a peak of 56.6 kips, approximately 690% of the SI service load or 422% of the SI ultimate load. The upgraded joist HJ-3 was then tested, and failed at a load of 52.6 kips, 393% of the ultimate SI design load. The two control joists, HJ-6 and HJ-7, failed at 48.7 kips and 65.0 kips respectively. HJ-6 failed at well below the anticipated capacity but still 363% of the ultimate SI service design load. The premature failure was attributed to insufficient shear reinforcement.

Deflection parameters, including camber at tendon release and experimental deflections due to the applied loads are summarized in Table 12. For the 31 ft clear span and 6 ft tributary width, the experimental deflections at the load equivalent to live load (LL), 3.5 kips, and the load equivalent to SI dead load (DL) + LL, 4.1 kips, are much lower than the ACI 318-95 limitations of L/360 (1.0 in.), and L/240 (1.55 in.), respectively, for specimens HJ-3 and HJ-4. Similarly HJ-6, and HJ-7 with 4 ft tributary widths deflected much less than the ACI limitations under loads of 2.3 kips and 4.0 kips for (LL) and (SIDL + LL), respectively. HJ-4 with the FRP repair permitted a midspan displacement of more than 11.3 in. without failing. The test was stopped as there was a lack of space to further deflect the joist. HJ-3 was able to deflect 7.7 in. before failure was initiated.

The experimental load versus midspan deflection curves for joists HJ-3, HJ-4, HJ-6, and HJ-7 are shown in Figure 19. Initial stiffness (below 0.2 psf) of all specimens is similar. After this point the stiffnesses of HJ-3 and HJ-4 were less than for either control joist. HJ-3 displayed more flexible response than the damaged or repaired joist HJ-4. HJ-4 was not able to achieve the performance of the control beam HJ-7 which had sufficient shear reinforcement. All joists were able to achieve their peak load repeatedly for several loading/unloading cycles. HJ-4 achieved the peak load for 5 cycles before the test was stopped. Its stiffness did not change significantly from cycle to cycle, Figure 20.

Deflection profiles along the joist length were approximated using potentiometer data as well as manual measurements from the joists' top flanges. A deflection profile is shown for HJ-3 with respect to load increments of a single actuator in Figure 21. Figure 22 shows deflection profiles for HJ-4 prior to repair and after the joist was repaired with FRP. HJ-3 deflected more than either the original or repaired HJ-4 for comparable load levels up to 25 kips. It also deflected much more than HJ-6. Similar plots for the other tested joists are shown in Figures 23 and 24. HJ-4, while able to deflect significantly was not able to match the performance of HJ-7. The shapes of HJ-3 and HJ-4 are much like that of the control joist, HJ-7. The shapes reflect the constant moment between load points and the

marked stiffness variation along the specimen length. The increased curvature with increasing load also reflects progressively greater cracking in the center section of the joists. The deflected shape of HJ-6 emphasizes the effects of insufficient shear reinforcement in the joist's inability to benefit from the prestressing and optimized shape.

Strains

Three types of strain readings were used in testing the family of hybrid joists: internal strain of reinforcement and external strain on FRP surfaces — both measured by strain gages — and displacement measured over a specified gage length on concrete surfaces by LVDTs. For the latter measurements cracks may have developed within the gage length, and the strain (displacement/displacement) may be greater than the maximum concrete strain range of 0.003 – 0.004 for compression or 0.0001 – 0.0002 for tension.

Strain distribution over section depth is shown in Figures 25 and 26 for three critical sections of HJ-3 and HJ-4 with FRP repairs. The distribution was approximated from concrete strain measurements near the top of the section and prestressing strand strains above and below the openings. Similar plots are shown in Figures 27 and 28 for HJ-6 and HJ-7, respectively. Strain along prestressing tendon length is shown in Figures 29 and 30 for HJ-3 and HJ-4 respectively. Figures 31 and 32 show strand strain measurements for HJ-6 through HJ-7.

Strains at the end and midspan of HJ-3 are similar in magnitude to those of HJ-6. It is apparent from Figure 25 that the full prestressing capacity could not be developed in these joists. This is further shown in Figure 29 where results of internal strain measurements along the strands for both top and bottom strands of repaired joist HJ-3 are presented. Strains in tendons were greatest in the shear span of this joist. In the constant moment region, strains are much less for both top and bottom tendons. From the strut section strain distribution, we can see that the neutral axis lies at a depth approximately 5 in. from the top of slab in HJ-3. From Figures 29 and 31 it is apparent that failure occurred before the full prestressing capacity could be developed in these joists.

Comparing Figures 26, 25, and 28, strain distribution in the repaired joist HJ-4 is quite different from that of either HJ-3 or HJ-7. The neutral axis indicated by the midspan strain is located at the member midheight. Peak strains in top and bottom prestressing strands of HJ-4 were greater than those in HJ-7, Figure 30 versus Figure 32. However, strain distribution over bottom tendon length is

much more uniform in HJ-7 providing greater ultimate flexural capacity of this section. HJ-4 did not approach the load capacity of HJ-7.

To assess the stress in the strands, the strains shown must be added to the strain due to prestressing and related to the elastic modulus of the material. The strand was fully tensioned, so the effective strain due to the prestress is approximately 6705 micro strain [(f_{se}/E_s) = 0.75 (270) / (30,000) (10^6) = 6750 micro strain]. All strains were below the ultimate strand strain of 35,000 micro strain. Again, the lack of strain developed in the strand indicates the poor performance of HJ-6. During testing it was observed that the bottom chord of HJ-7 appeared to arch upward between the struts; this may be related to the larger strains shown at the struts than the midspan for some load levels.

Figures 33 and 34 show load versus strain in the FRP material for HJ-3 and HJ-4 respectively. Strain gages along the beam web show elongation of transverse FRP with increasing load. In HJ-4 FRP strains do not begin to increase appreciably until the actuator load is approximately 12 kips indicating the widening of shear cracks in the concrete beneath the FRP and the developing shear resistance in the FRP. Strain in gages ES4 and ES5, closest to the beam center, reached a peak value greater than 0.005 in./in. This is above the allowable strain of 0.004 but much less than the ultimate strain of 0.02. The limited capacity of HJ-3 is shown by the much lower strain values of gages ES4 and ES5 than for HJ-4.

Cracking and Failure Mechanism

None of the joists cracked when the prestressing tendons were released. During handling, specimen HJ-7 developed a crack across the slab through its depth near the south strut. Cracks were marked on each of the joists throughout testing. Cracking and failure mechanisms resulting from testing of HJ-6 and HJ-7 were compared with those of the two hybrid joists upgraded or repaired with FRP. Early in the test series, limited cracking occurred in the bottom chord of HJ-6. As actuator stroke was increased, cracking in the shear spans became evident but the cracks in the bottom chord did not develop further. In HJ-6 an inclined crack developed near the support and progressed upward along the web/slab interface (Figure 35). This crack progressed into the slab and failure ultimately occurred in this North end of the joist (Figure 36).

Figure 37 shows crack development for HJ-7. Initial flexural cracks formed along the bottom chord at midspan. Cracks were regularly spaced, and they became more numerous and closely spaced as the displacement was increased. Near the end of testing, when the load was not increasing but the specimen was

able to deflect significantly more, inclined cracks developed in the shear spans of the members. No actual failure was observed in specimen HJ-7. The joist continued to deflect after reaching an ultimate load capacity.

Cracking in HJ-3 initiated as for HJ-7 with flexural cracks in the web bottom chord. At an applied stroke of approximately 5 in. a crack began to develop along the edge of the FRP at the intersection between the joist web and slab, Figure 38(b). A gap of more than 1 in. of exposed concrete existed where the FRP had slipped down from the web/slab interface. The horizontal crack began near the point where the FRP lapped. As the horizontal crack progressed toward the North end of the joist, cracks also developed in the bottom of the slab perpendicular to the joist span as well, Figure 38(a). These were associated with popping sounds as if the FRP were debonding from the joist. A vertical crack in the FRP was observed at a distance approximately 6 in. from the north end of the joist. This occurred at a stroke of approximately 7.5 in. A maximum deflection of approximately 9 in. was achieved before complete collapse of the joist occurred by fracture of the top slab at a distance of approximately 56.75 in. from the north end. The FRP separated from the joist by buckling over the web depth at a distance approximately 41 in. from the joist north end. A third vertical break in the FRP was observed at 25.5 in. from the end, Figure 39 (a). These cracks in the FRP were accompanied by peeling of the top slab from the web at the construction joint, Figure 39 (b). Investigation of the failure revealed the concrete in the area of the FRP repair had completely broken up. The total length of crumbled concrete was approximately 50 in. Examination of the TYFO™ S Fibrwrap System showed it to be adhered to the perimeter concrete even at failure. Failure was in the concrete. This was precipitated by the weakness created by the gap in the FRP repair at the top of the web.

Initial testing of HJ-4 without FRP repair produced crack patterns similar to those for HJ-6, Figure 40. After repair testing began again, existing cracks between struts increased in size and additional cracks were observed to develop near the edge of the FRP repair area, Figure 41 (a) and (b). The test had to be stopped when there was no further vertical space between the web bottom chord and the floor for the joist to deflect. The joist did not fail. At the test conclusion, the FRP repair showed no signs of damage. The beam exhibited ductile response throughout the test.

Experimental Test Conclusions

HJ-4, while being damaged prior to application of the FRP repair, was able to deflect as much as HJ-7. However HJ-4 with FRP repair was not able to achieve the strength and stiffness levels of a properly reinforced specimen, HJ-7. The

shear mode failure of HJ-3 was initiated by a gap on the joist web where the FRP
had slipped during curing. Its performance was not improved over HJ-6.

4 Design Procedure for Hybrid Joists

Overview

Based on standard structural engineering design principals and the experimental test results, a simple procedure was developed to design FRP composite system repairs for reinforced concrete joists deficient in shear capacity. This design procedure is a step-by-step process wherein load demands are assessed for an existing member cross-section, a repair is designed based on specified engineering properties of the FRP composite system to achieve the required capacity, and stresses and deflections for the repaired joist are checked. Figure 31 shows the flowchart for the joist design procedure.

Design Criteria and Assumptions

Design criteria are based on *Building Code Requirements for Reinforced Concrete*, ACI 318-95 (1995). Load and strength reduction factors as specified by the code are used. Flexural strength is calculated using strain compatibility.

The International Conference of Building Officials has developed a draft document on the subject of "Acceptance Criteria for Concrete and Reinforced and Unreinforced Masonry Strengthening Using Fiber-reinforced Composite Systems" (ICBO 1997). This document provides good guidance for the establishment of minimum requirements for evaluating FRP systems for strengthening concrete elements.

The joist is assumed to be uniformly loaded at all stages with a simple span and roller supports.

Design Procedure

Define Loading

As stated above, uniform loading of the beam is assumed. Service loading is defined as the unfactored load. This will generally be a combination of the beam

self-weight, superimposed dead load, and live load. Ultimate load is typically defined as shown below:

Ultimate Load = 1.4 DL + 1.7 LL

where: DL is the sum of the self-weight and superimposed dead load and

LL is the live load

Calculate the service load for each loading stage. Calculate the ultimate loads acting on the joist. Again, it must be noted that the CPAR test results do not support the use of this type of hybrid joist where concentrated loads will be applied.

Define Capacity of Existing Beam Section

Flexural and shear capacity of the section should be computed without use of reduction factors based on the existing properties.

Flexural capacity is based on strain compatibility and equilibrium. A maximum concrete compressive strain of 0.003 is being assumed. The ultimate moment capacity, M_u is computed as:

$$M_u = A_s f_y \left(d - \frac{a}{2} \right)$$

where: $a = \dfrac{A_x f_y}{0.85 f_c' b}$

and a = depth of equivalent rectangular stress block, in.

A_s = the area of flexural reinforcement, in.^{2}

f_y = yield stress of reinforcement, ksi

d = distance from extreme compression fiber to extreme tension steel, in.

f_c' = compressive strength of concrete, ksi

b = section width, in.

Shear capacity is a function of the concrete shear strength and shear reinforcement:

$$V_n = V_c + V_x \qquad \text{(ACI, 1995 Equation 11-2)}$$

where V_c is nominal shear strength provided by concrete computed as:

$$V_c = 2\sqrt{f_c'}\, b_w d \qquad \text{(ACI, 1995 Equation 11-3)}$$

for members subjected to shear and flexure only. If the beam has been damaged a conservative assumption of the concrete shear capacity is $V_c = 0$.

V_s is nominal shear strength provided by shear reinforcement and computed as:

$$V_s = \frac{A_v f_y d}{s} \qquad \text{(ACI, 1995 Equation 11-15)}$$

where A_v is the area of shear reinforcement within a distance.

Determine Load Requirement for Upgrade/Repair

The degree of upgrade/repair required is represented by the difference between the load demand and the existing section capacity. The ratio of shear capacity to shear demand should exceed that of the flexural capacity to flexural demand. This is to ensure that a shear failure mode, which can occur without warning and may be catastrophic, does not occur. Rather a ductile mode of failure with obvious signs of distress, as would occur in a flexural failure, is desirable. The final shear capacity of the upgraded/repaired beam should be approximately 1.5 to 2.0 times the flexural capacity. The upgrade/repair demand will be represented as V_{req} - required additional shear capacity.

Determine FRP Properties

Shear enhancement is provided by fiber-reinforced composite materials with fibers oriented essentially perpendicular to the member's axis. Fiber orientation is critical when determining FRP properties. Important properties to define for design are:

f_{sj} , allowable FRP tensile stress

f_{uj} , ultimate FRP tensile stress

σ_j , allowable bond stress

E_j , FRP modulus of elasticity

ε_{aj} , allowable FRP strain

ε_{uj} , ultimate FRP strain

ICBO limits allowable composite material stress, f_{aj} , to be $0.004\,E_j$ and less than $0.75\,f_{uj}$.

Determine Configuration and Calculate Thickness of FRP

Research directed toward determining effective configurations of FRP shear repairs for beams by Al-Sulaimani et al. (1994) showed that the use of strips or wings on the beam faces provided comparable increases in shear capacity. However, the mode of failure for these sections tested was still in shear. Shear repair by a jacket on three sides performed better than repair by strips or wings. The wings of the jacket were well anchored at the bottom of the beam so that no premature peeling failure occurred. Additionally the continuity provided by the geometry of the jacket minimized the effect of stress concentrations in the plates. The beams repaired with FRP jacket exhibited a higher capacity than those of the strip or wing upgrade and ultimately failed in flexure.

A jacket configuration should, therefore, be assumed whenever possible. It is optimal to wrap the entire section in the FRP. If this is not possible the use of anchors should be considered so that bond is not the primary mechanism of force transfer.

Assuming a layer thickness of t_j .

$$V_{req} = 2t_j f_{aj} H \sin\theta$$

where H is the depth of the FRP and θ is the angle of the fibers relative to the member axis. This equation assumes a shear crack inclination of 45 degrees. ICBO recommends the following equation:

$$V_{req} = 2.86 t_j f_{aj} H \sin^2\theta$$

Check Stresses

Bond, flexural, and shear stresses should be checked for the upgraded/repaired joist configuration.

Check stresses due to service loads.

Check stresses at ultimate loading using ACI 318-95 approximate equations or the strain compatibility method:

$$V_u = V_c + V_s + V_p$$

where: V_u, V_c and V_s are defined above and V_p is computed as

$$V_P = 2F_P = 2\left[\sigma_{uj}\left(\frac{dH}{2}\right)\right]$$ (Al-Sulaimani et al. 1994)

This equation assumes a full U-jacket is used, that shear distribution is uniform over the depth of jacket, with the absence of stress concentrations; therefore, the ultimate stress of the material may be achieved.

Check bond shear stress. ICBO guidance requires that where the performance of the composite material depends on bond, the bond strength of fiber-reinforced composite material to concrete [u_j] shall not be less than the characteristic flexural tension capacity f'_t of the concrete. Under ultimate flexural strength conditions, bond stress between fiber-reinforced composite material and concrete shall not exceed:

$$u_j = \frac{d\left(t_f f_j\right)}{dx} \leq 0.75 f'_t$$

where x is the direction parallel to the fiber. This value should be evaluated at sections where the rate of change in fiber net force, $t_f f_j$, is a maximum. This will normally correspond to locations of maximum shear force.

Check Deflections

An estimate of the load deflection relationship should be checked using structural analysis methods. Deflection limits should be evaluated relative to ACI code requirements.

Determine Failure Mode

The member should be designed to fail by ductile flexural failure mode. For the strengthening of existing reinforced concrete beams with FRP it is recommended that the repair/upgrade be designed such that ultimate failure occurs by yielding of the steel reinforcing bars before a compressive failure of the concrete. Yielding of the steel bars should not occur before reaching the permitted service loads.

Detailing

For rectangular sections where shear enhancement provided by transverse fiber-reinforced composite material, section corners must be rounded to a radius not less than ¾ in. (20mm) before placement of the composite material.

Design Example

Assumptions

The concrete weight is 150 pcf.

Concrete compressive strength is 4 ksi,

Steel reinforcement yield stress is 60 ksi.

Shear reinforcement consists of #3 U-stirrups at 6 in. o.c. over the length of the beam.

FRP Properties

Beam is originally designed to carry 4 k/ft uniform load. Check shear capacity.

$$V_u = \frac{4 \times 25}{2} = 50 \text{ kips}$$

Shear at critical section (at distance d from end) by similar triangles:

$$V_u \text{ at d} = \frac{50 \times (12.5 - 1.5)}{12.5} = 44 \text{ kips}$$

$$V_u < \phi V_n$$

where: $\phi V_n = \phi V_c + \phi V_s$

$$V_c = 2\sqrt{f'c}\, b_w d = 2\sqrt{4000}\,(12)(18) = 27.3 \text{ kips}$$

$$V_s = \frac{A_v F_y d}{s} = \frac{(0.22)(60)(18)}{6} = 39.6 \text{ kips}$$

$\phi V_n = (0.85)(27.3+39.6) = 56.7 \text{ kips} > 44 \text{ kips } \textbf{OK}$

$$\text{Minimum: } A_v = 50\frac{b_w s}{F_y} = \frac{(50)(12)(6)}{60000} = 0.06 \text{ in}^2$$

A_v (provided = 0.22 in^2) > A_v (required = 0.06 in^2) **OK**

Now, suppose uniform load increases to 6.5 k/ft.

V_u at critical section = 71.5 kips

Shear deficiency = 71.5 - 56.7 = 14.8 kips (say 15 kips)

We need FRP wrap from end to point along beam where shear is less than 56.7 kips.

$$x = \frac{(56.7)(11)}{71.5} = 8.72 \text{ feet (say 9 feet)}$$

Requires FRP wrap from end to 9 feet

Using Fibrwrap™ Jacket and TYFO TC epoxy adhesive

$$V_{req} < 2t_j f_{sj} d\cot 45°$$

where: $t_j = 0.051$ inches (jacket thickness)

$f_{sj} = 12$ ksi (allowable jacket stress)

and assuming 45° crack inclination

$$\text{number of jackets} = \frac{15}{2(12)(18)(1)(0.051)} = 0.68 \text{ (1 layer required)}$$

check bond stress: $\quad u = \dfrac{15}{(18)(9 \times 12)} = 8$ psi < 400 psi allowable **OK**

Compute material required assuming a U-shaped jacket wrap.

Surface area = 2ends(8"+8"+5")(48") = 2496sq.in x 2 layers ---> 34.7 sq.ft

Surface area = 2ends(24"+24"+5")(48") = 14384sq.in x 2 layers ---> 200 sq.ft

5 Conclusions and Recommendations

The results of tests performed in this study indicate that significant increase in shear strength can be achieved by the application of FRP to concrete beams deficient in shear capacity. When an FRP jacket is properly applied over the shear span of the member the failure mode of a member may be altered from that of a brittle shear failure to a ductile flexural failure mode. However, the repaired joist was not able to achieve the strength and stiffness levels of a properly reinforced specimen.

The effectiveness of an FRP upgrade or repair requires careful preparation of concrete surface, selection of a tough epoxy, and placement of the fabric. A gap between the web and slab that was not covered by the FRP proved to initiate failure in a joist upgraded with FRP. While the joist deflected significantly more than a control beam that failed in shear the mode of failure was similarly sudden and brittle. This joist's overall stiffness was not as great as for the two control joists. Bond between the FRP and concrete was shown to be very good.

Connectivity between the joist web and slab were also shown to be very important as all test joists tended to separate along this interface after testing was completed. Both joists that failed in shear failed along this interface. Insufficient shear reinforcement may also affect the quality of tendon anchorage, concrete confinement, and anchorage of the web to the cast-in-place slab. Proper application of FRP can assist in providing the latter two of these requirements but will not aid in anchoring prestressing tendons.

When designed or repaired with adequate shear reinforcement, the behavior of the test joists was exceptional. Failure loads for specimens HJ-4 and HJ-7 were very high compared with design service and ultimate loads. Failure was also very ductile for these members, with deflection capacity extending well beyond the point at which the ultimate load was reached. The hybrid joist behaved very much like a traditional prestressed precast concrete beam except that the hybrid system had the capability to carry 30% more load than the conventional prestressed double tee before first cracks appeared.

Additional analytical and experimental studies should be undertaken to establish the benefits of supplemental anchorage for improving the bond of the FRP to the reinforced concrete structural member. Construction methods for ensuring

proper placement and curing of the FRP in the repair process should be refined. In addition, the effects of environmental factors, e.g., temperature and moisture on the epoxy joint, as well as the performance of upgraded beams under fatigue loading should be examined.

References

American Concrete Institute (ACI). (1995). "Building code requirements for reinforced concrete and commentary." ACI 318-95, Detroit, Michigan.

Al-Sulaimani, G.J., A. Sharif, I.A., Basunbul, M.H. Baluch, and B.N. Ghaleb, "Shear Repair for Reinforced Concrete by Fiberglass Plate Bonding," *ACI Structural Journal*, vol 91, no. 3, (July-August 1994), pp 458-464.

Chajes, M.J., W.W. Finch, T.F. Januszka, and T.A. Thomson, "Bond and Force Transfer of Composite Material Plates Bonded to Concrete," *ACI Structural Journal*, vol 93, no. 2, (March-April 1996), pp 208-217.

Chajes, M.J., T.F. Januszka, D.R. Mertz, T.A. Thomson, and W.W. Finch, "Shear Strengthening of Reinforced Concrete Beams Using Externally Applied Composite Fabrics," *ACI Structural Journal*, vol 92, no. 3, (May-June 1995), pp 295-303.

Chajes, M.J., T.A. Thomson, and B. Tarantino, "Reinforcement of Concrete Structures Using Externally Bonded Composite Materials," *Non-Metallic Reinforcement for Concrete Structures (Proceedings)*, (1995), E&FN Spon, London, pp 501-508.

Engineered Materials Handbook, Volume 1, "Composites," ASM International, Metals Park, OH, (1987), p 36.

Gee, Duane J., Memorandum of 21 June 1996.

International Conference of Building Officials Evaluation Service, Inc., "Acceptance Criteria for Concrete and Reinforced and Unreinforced Masonry Strengthening Using Fiber-reinforced Composite Systems," AC125, (April 1997).

Norris, T., H. Saadatmanesh, and M.R. Ehsani, "Shear and Flexural Strengthening of R/C Beams with Carbon Fiber Sheets," *ASCE Journal of Structural Engineering*, vol 123, no. 7, (July 1997).

Saadatmanesh, H. and M.R. Ehsani, "Fiber Composite Plates Can Strengthen Beams," *Concrete International*, vol 12, no. 3, (March 1990), pp 65-71.

Figures and Tables
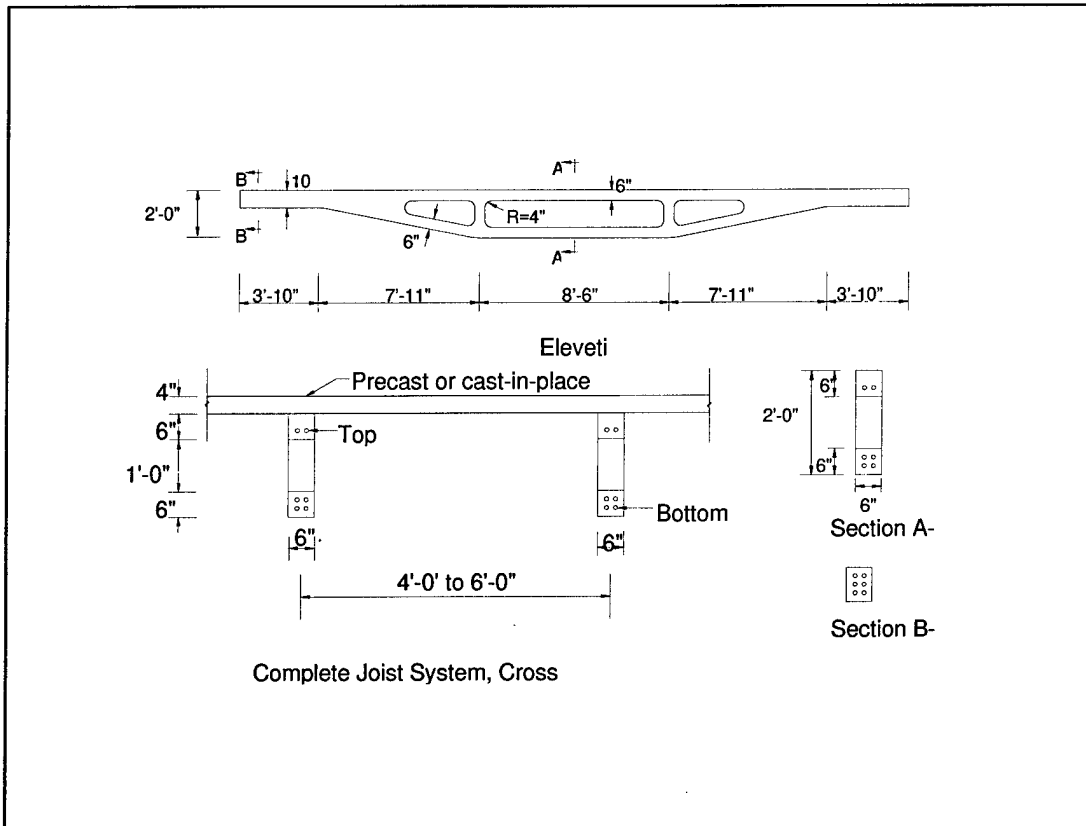
Figure 1. Joist configuration.
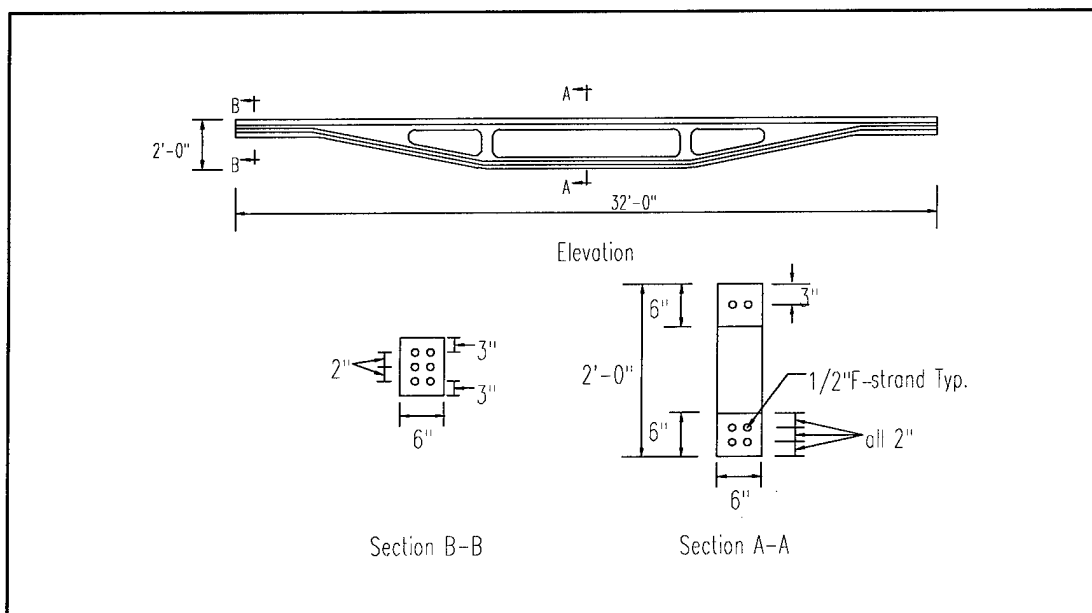
Figure 2. Joist prestressing tendon profile.
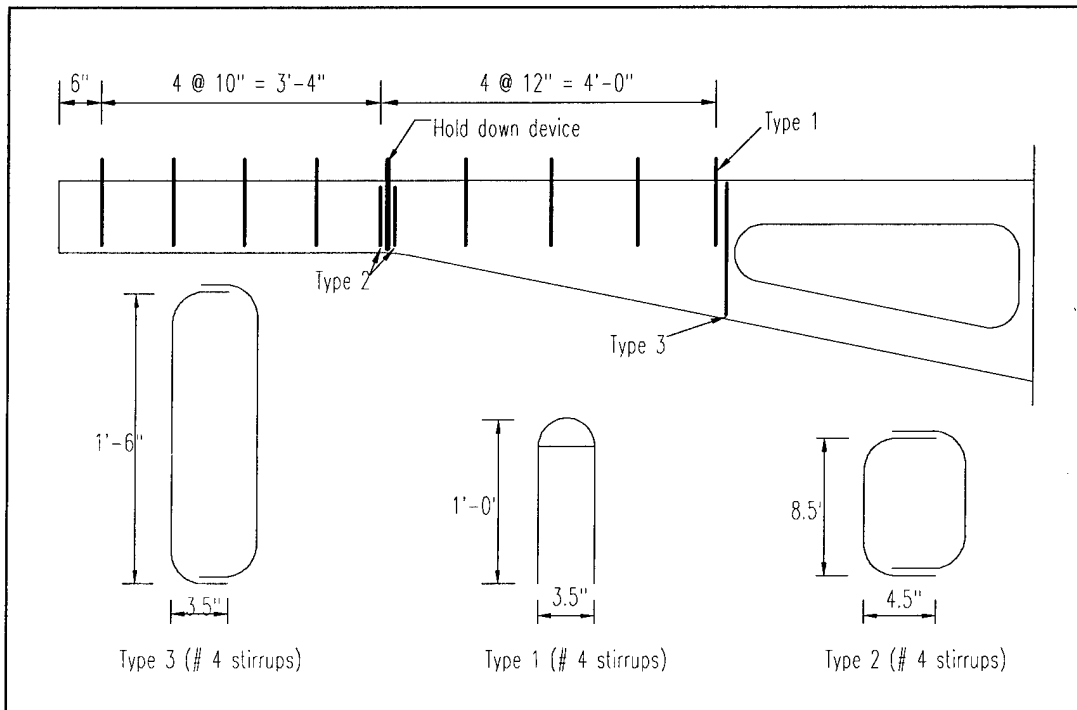
Figure 3. HJ-3 and HJ-4 web reinforcement.

Figure 4. FRP joist repair.
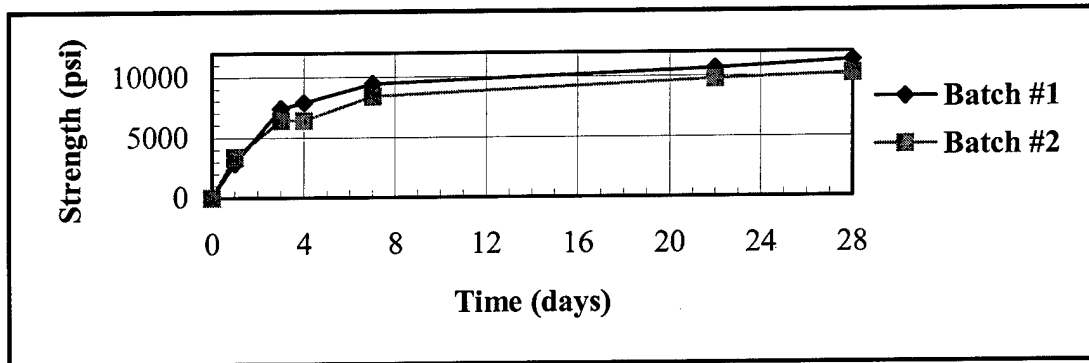
Figure 5. High-performance concrete strength versus time.
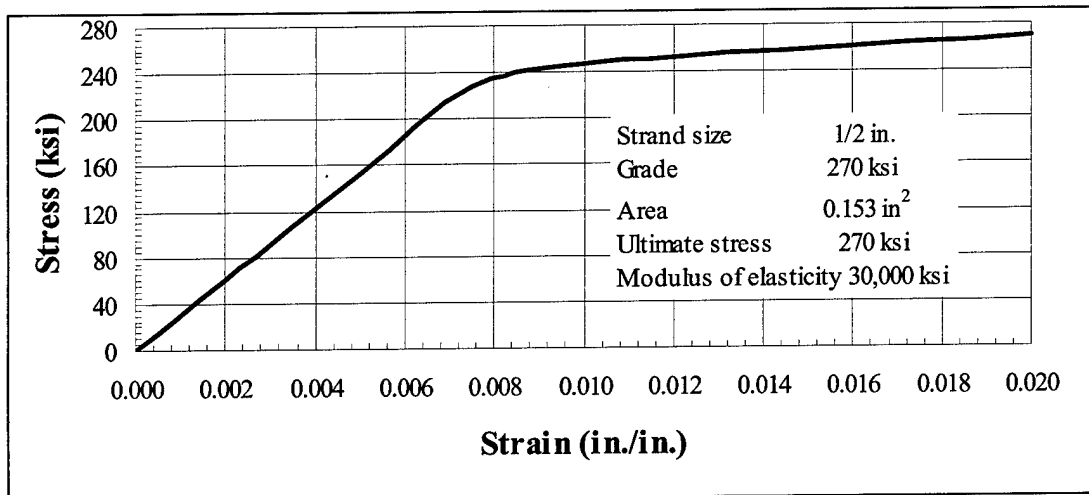
Figure 6. Prestressing tendon stress versus strain.
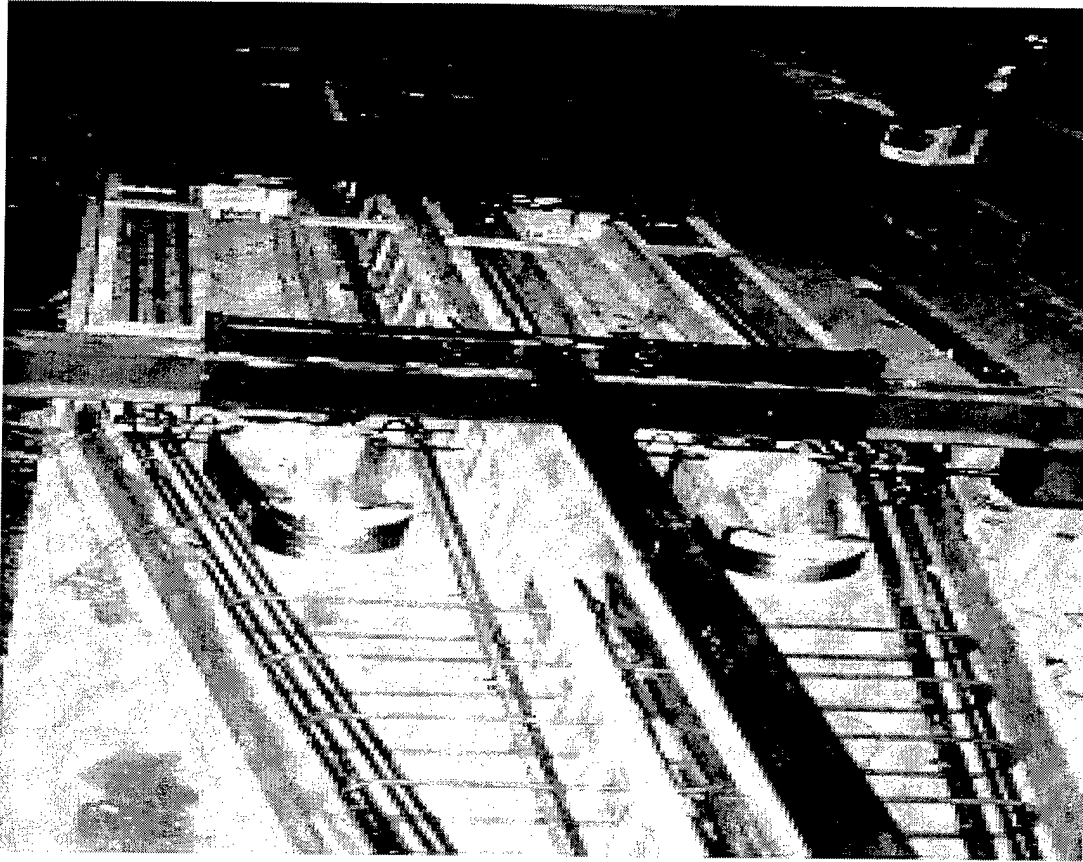
Figure 7. Prestressing and casting of hybrid joists.
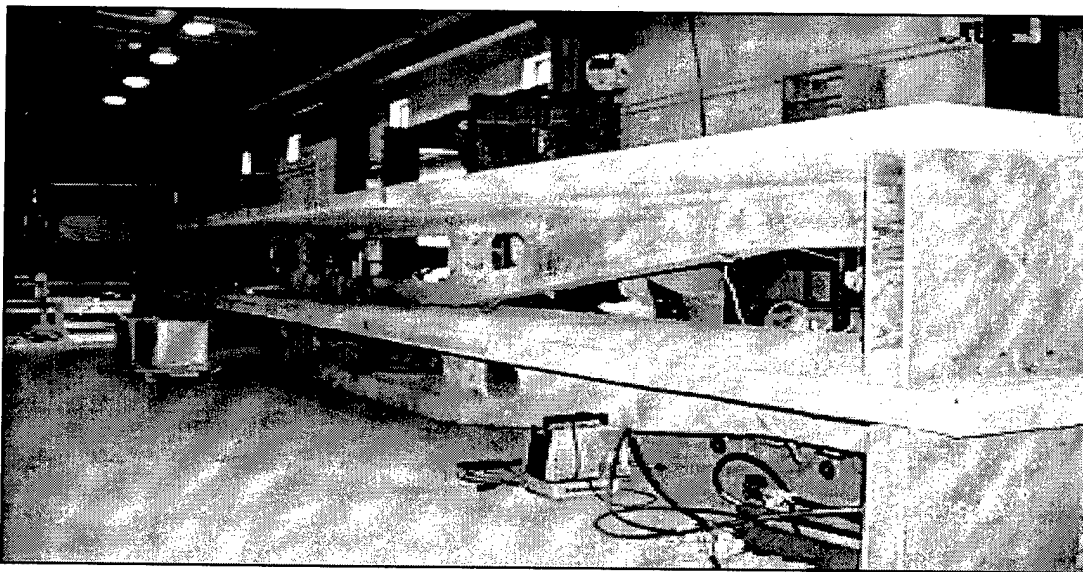
Figure 8. Completed hybrid joist construction.

Figure 9. FRP application.

Figure 10. Gap in FRP upgrade of HJ-3.

Figure 11. Epoxy injection of voids.

Plan view for the two joists

Note: Gages # 42, 43, 44, and 45 on the closed stirrups.
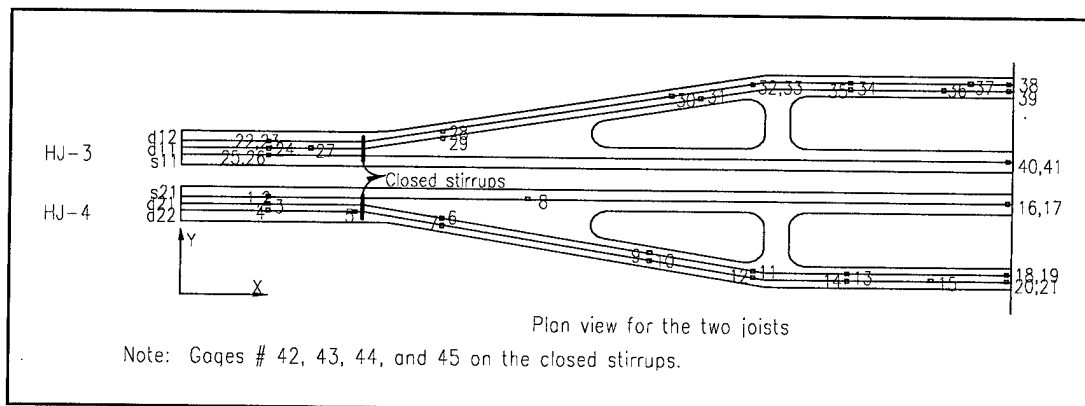
Figure 12. Internal strain gage layout for HJ-3, HJ-4, HJ-6, and HJ-7.
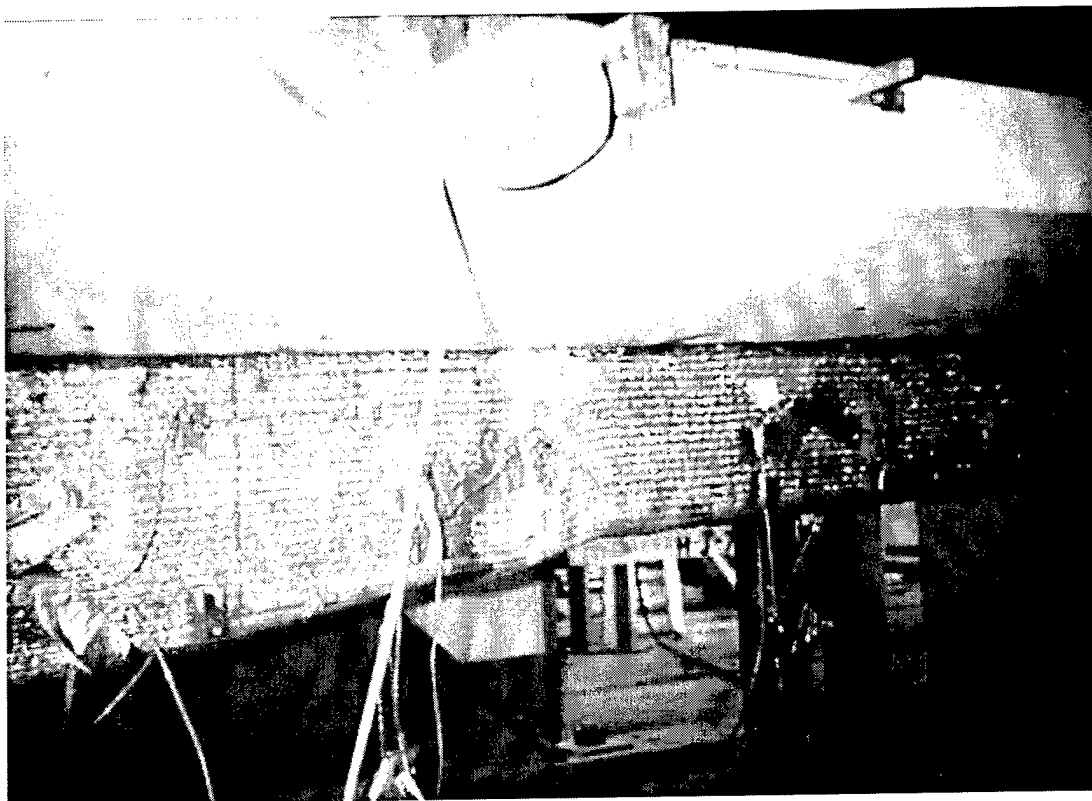
Figure 13. External strain gage layout on HJ-3.
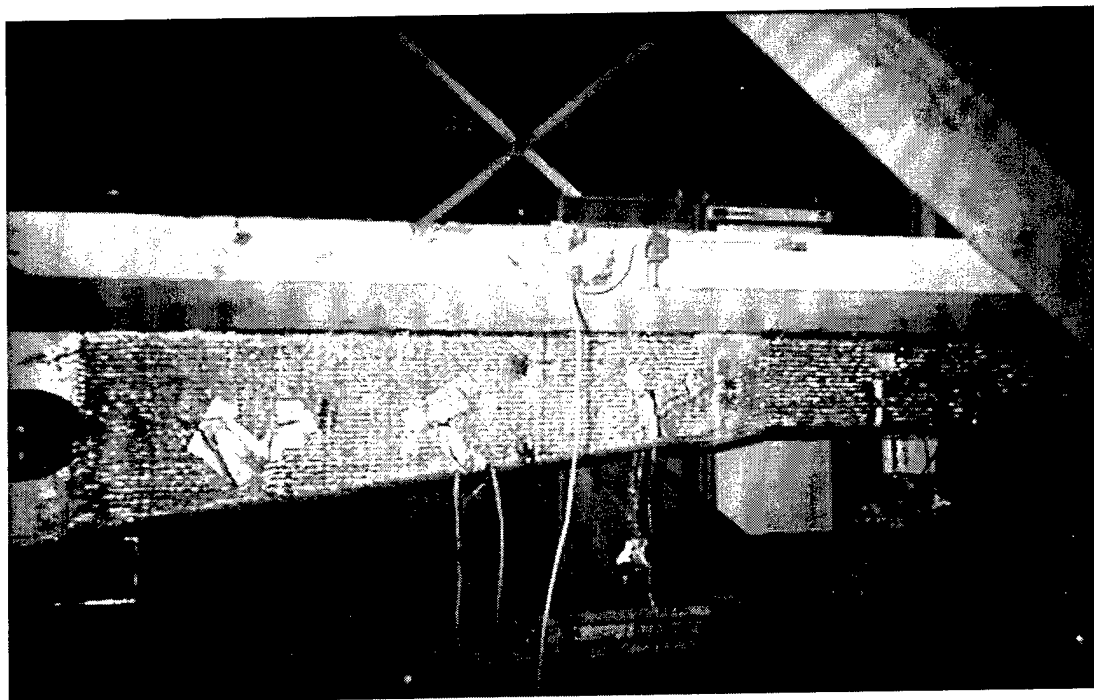
Figure 14. External strain gage layout on HJ-4.
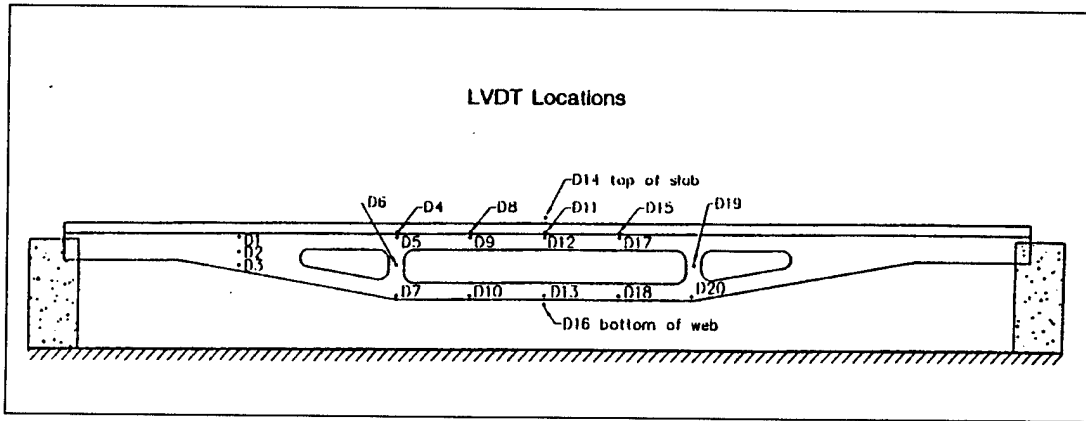
Figure 15. LVDT locations on test specimens.
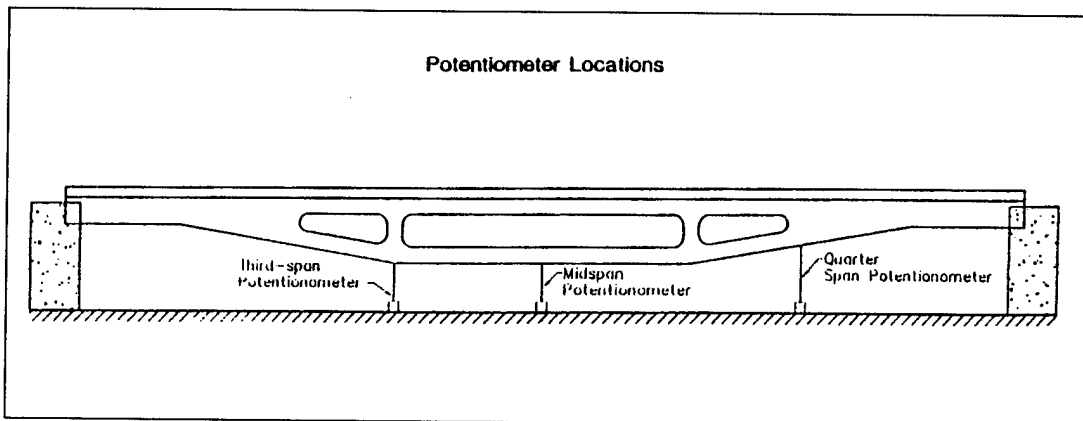
Figure 16. Potentiometer locations on test specimens.
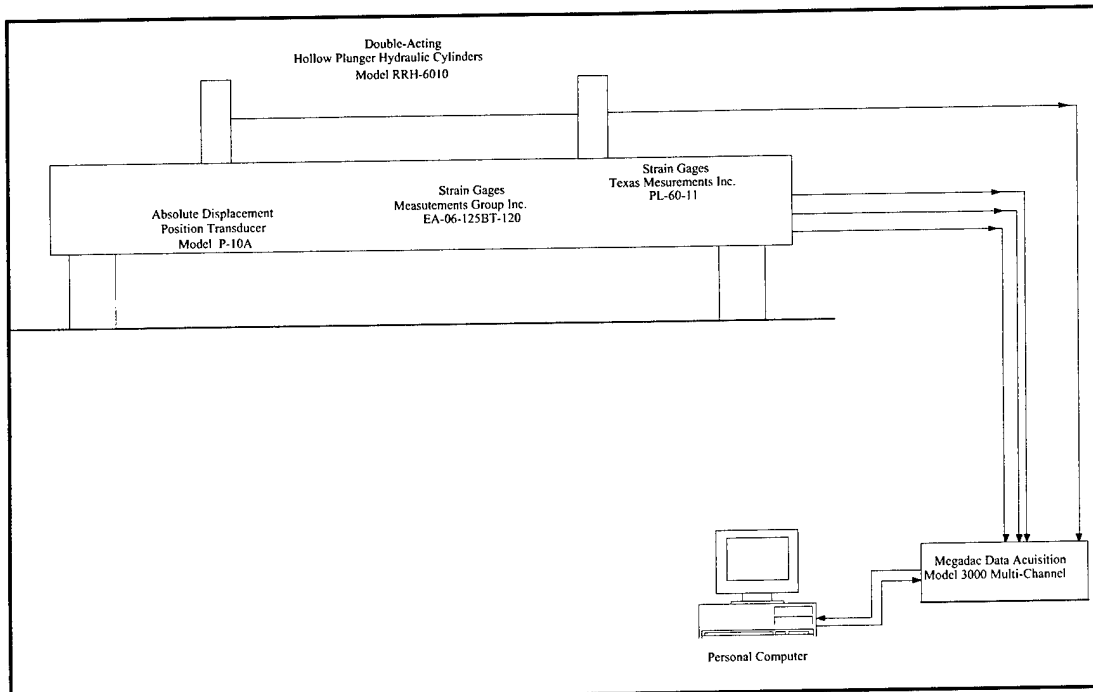
Figure 17. Block diagram of data recording system.
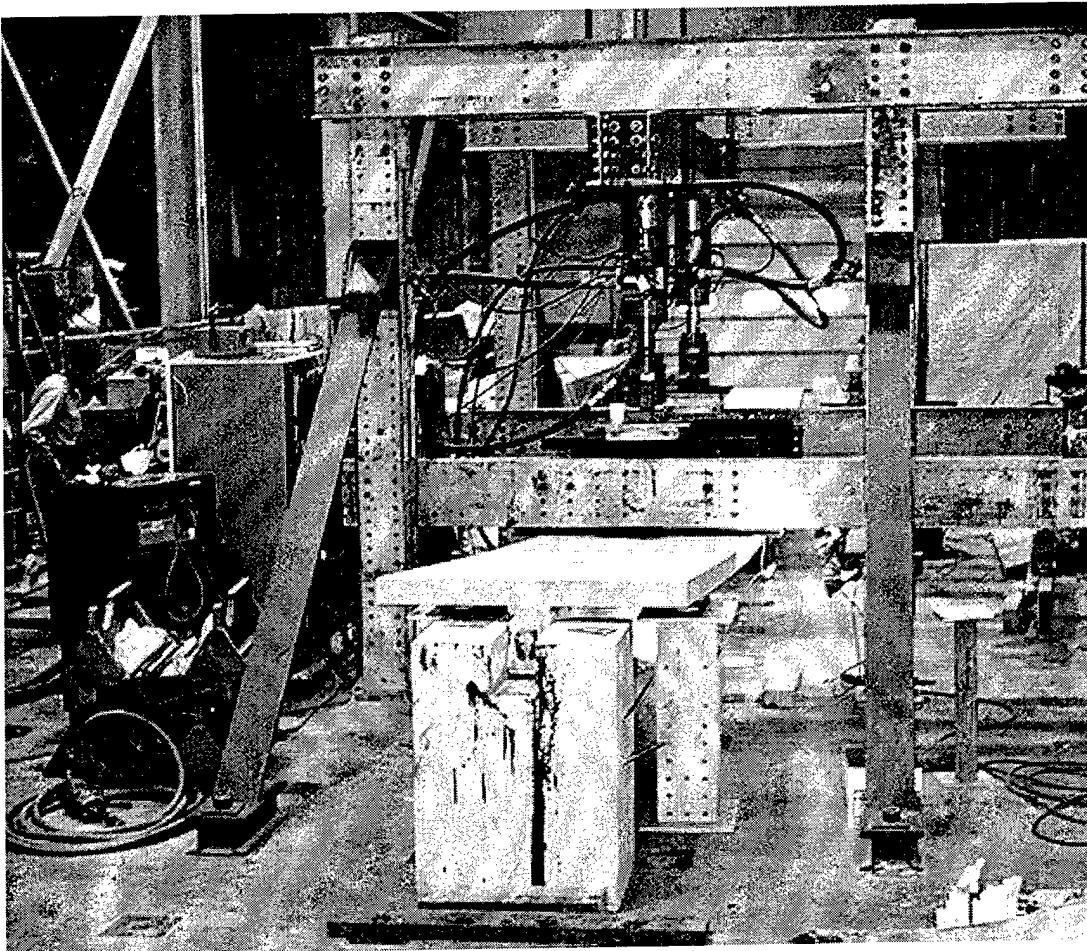
Figure 18. Test setup.
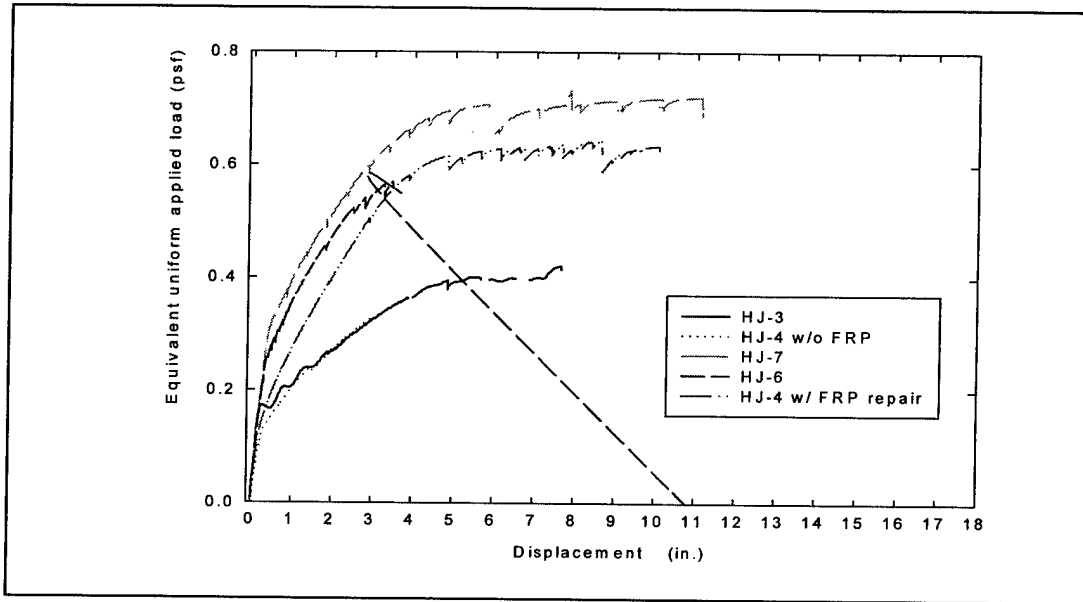
Figure 19. Load versus deflection for HJ-3, HJ-4, HJ-6, and HJ-7.
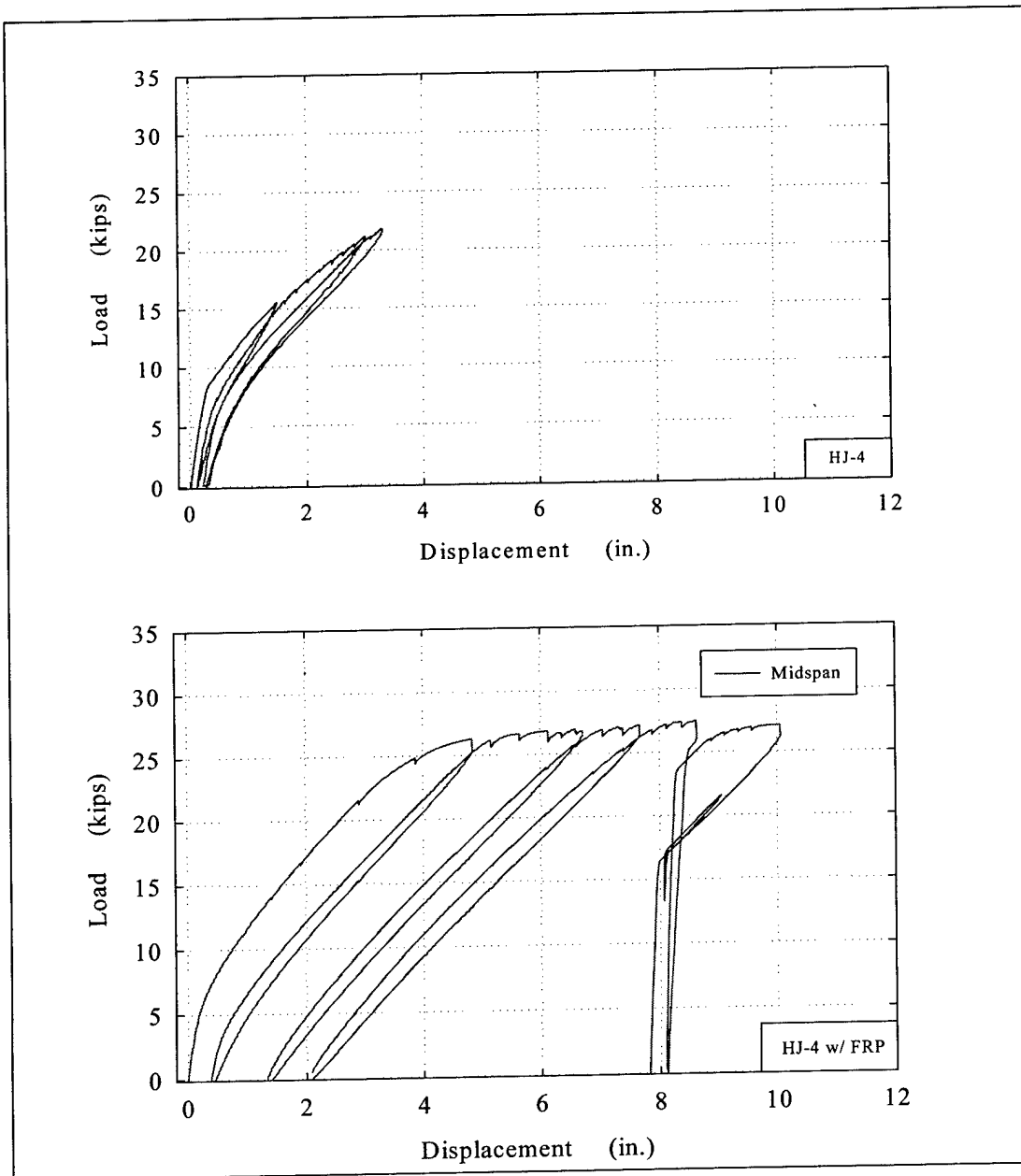
Figure 20. Load versus deflection cycles for HJ-4.
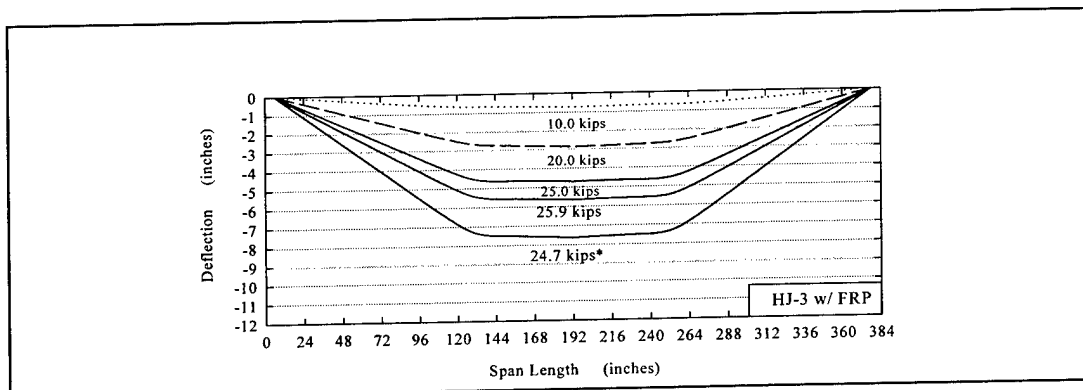
Figure 21. Deflected shape for HJ-3.
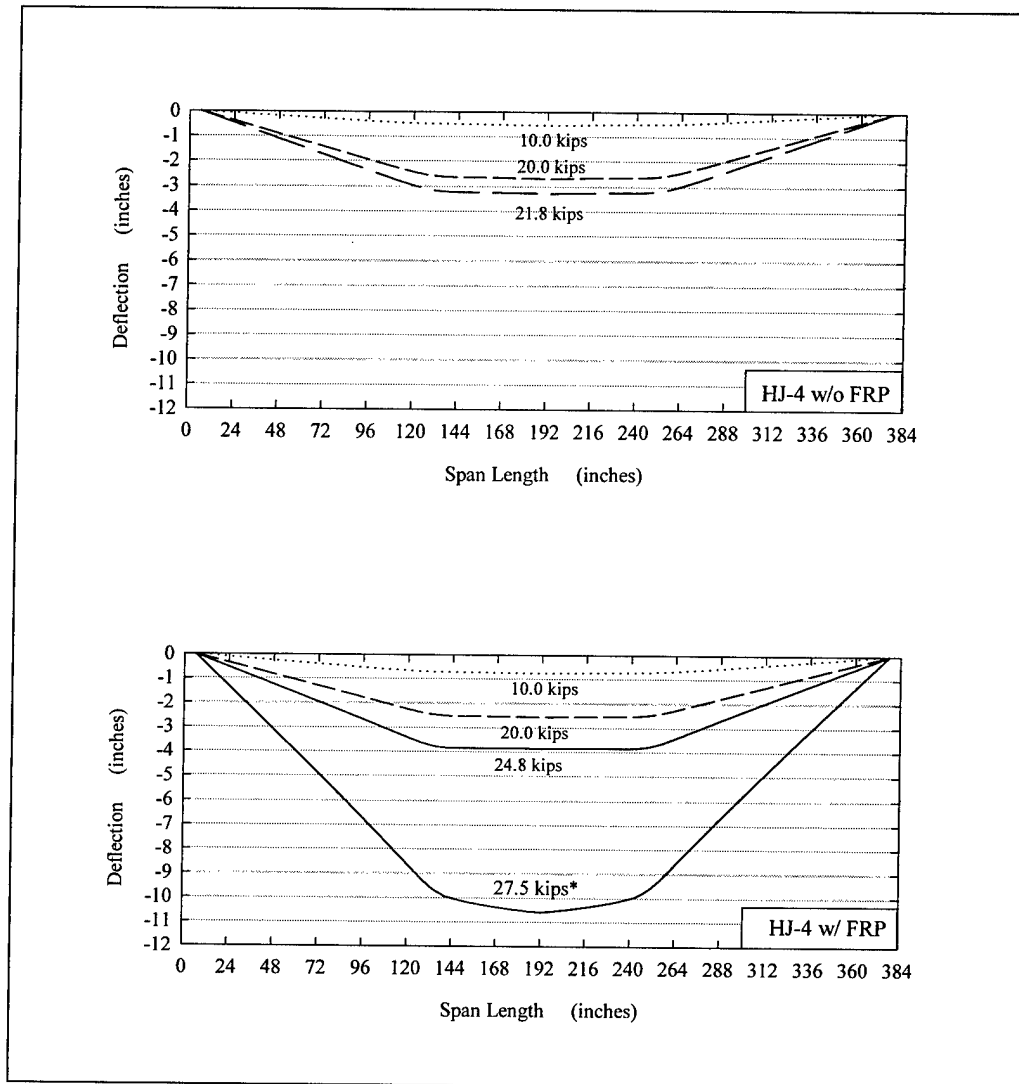
Figure 22. Deflected shape for HJ-4 before repair (top) and after FRP repair (bottom).
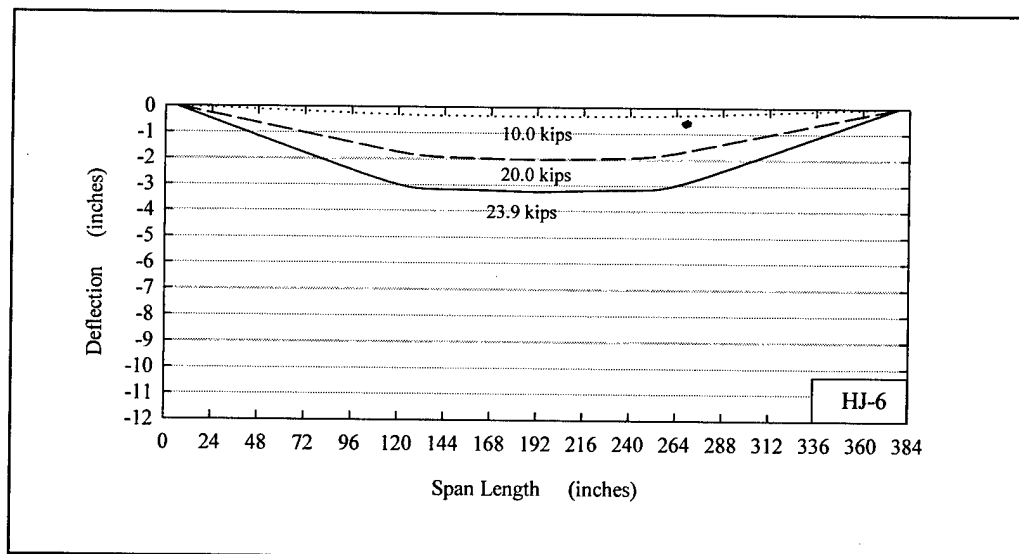
Figure 23. Deflected shape of HJ-6.
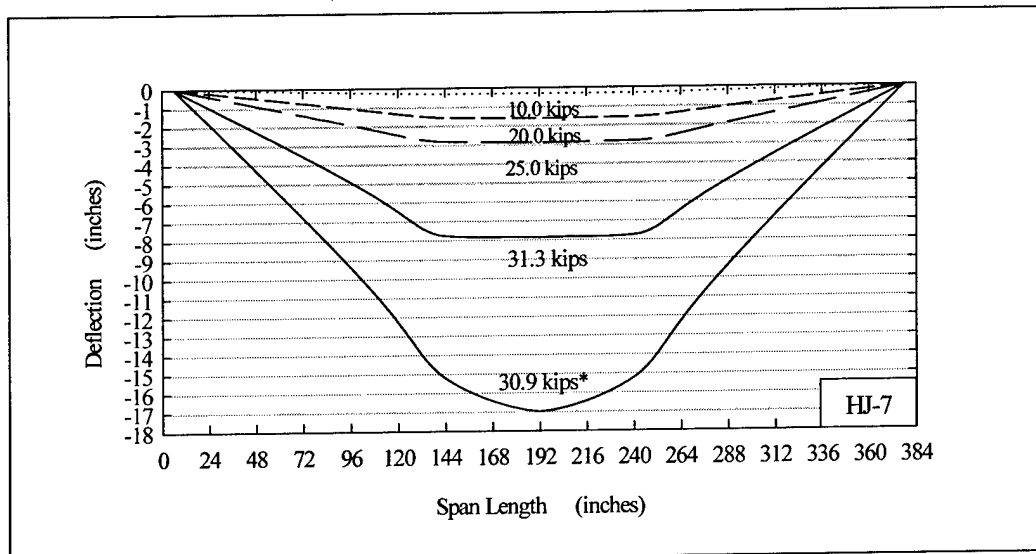
Figure 24. Deflected shape for HJ-7.
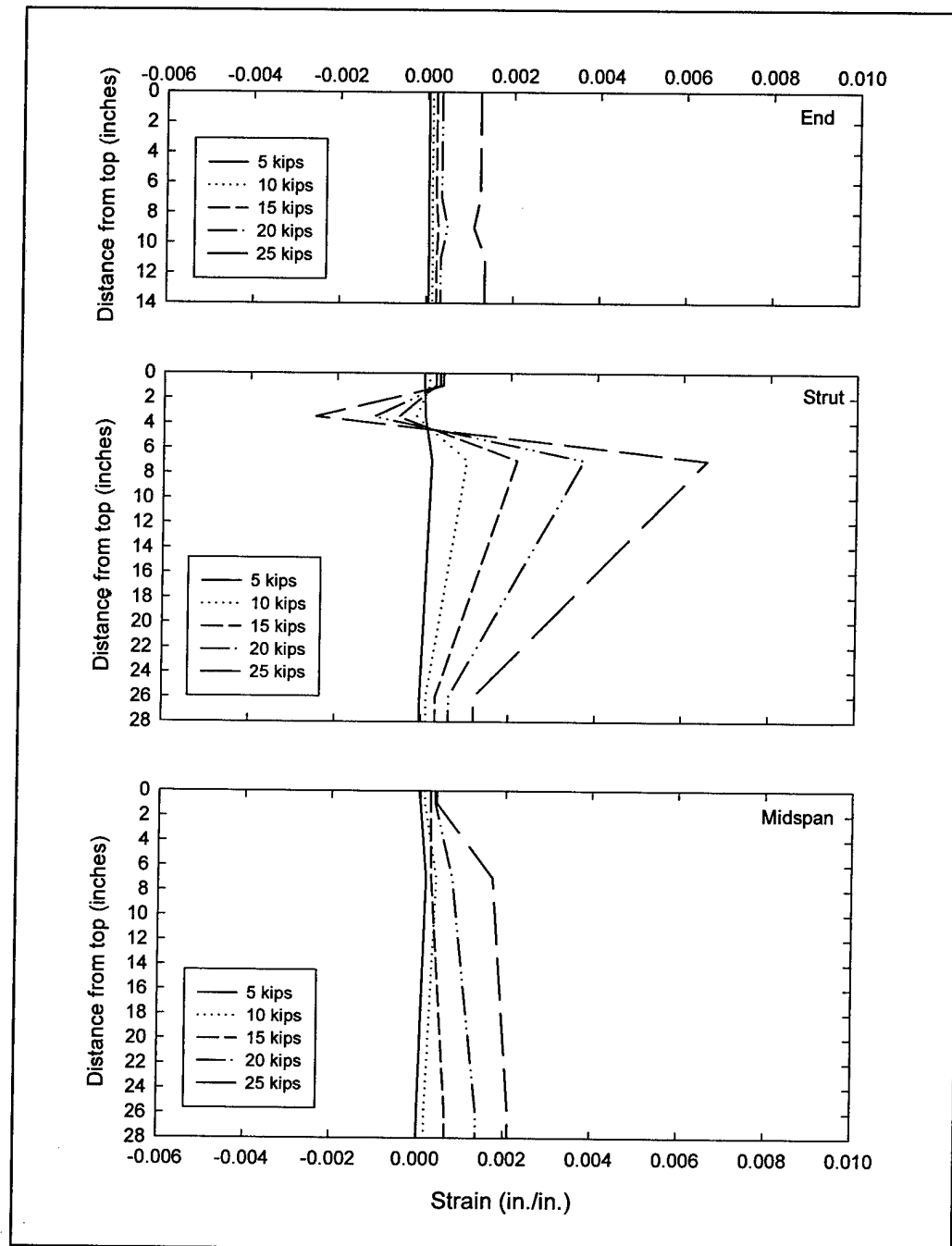
Figure 25. Strain distribution for HJ-3.
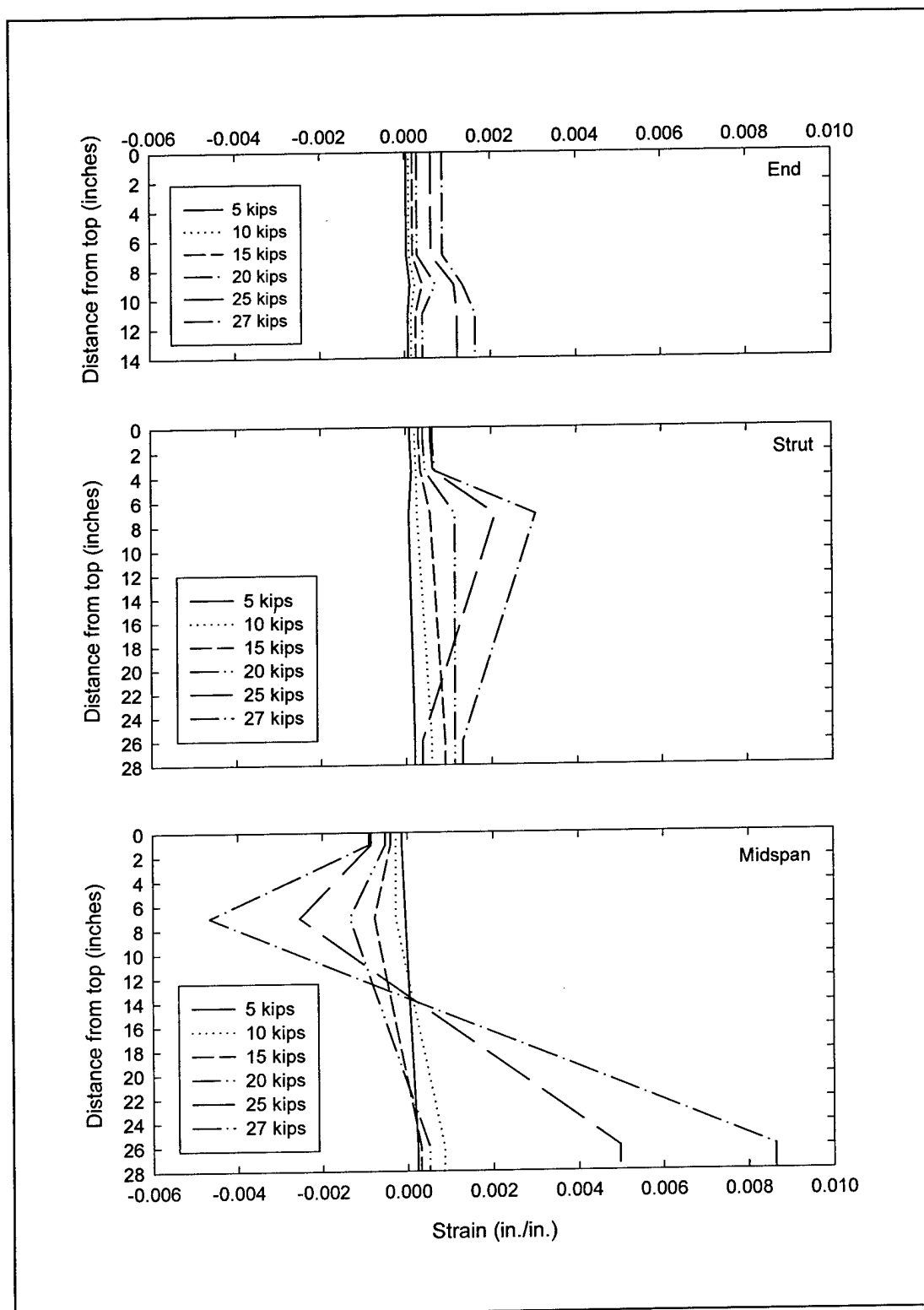
Figure 26. Strain distribution for HJ-4.
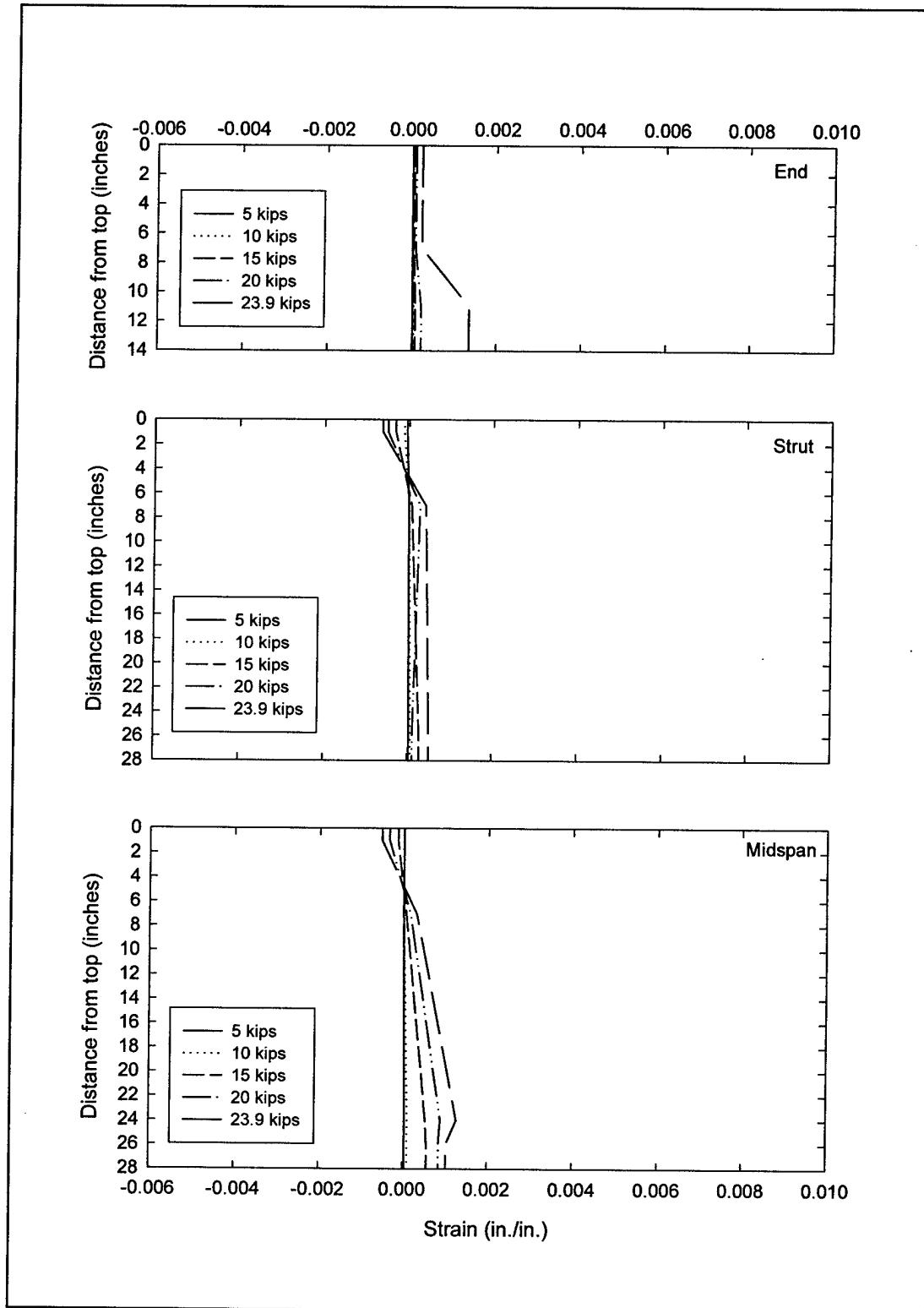
Figure 27. Strain distribution for HJ-6.
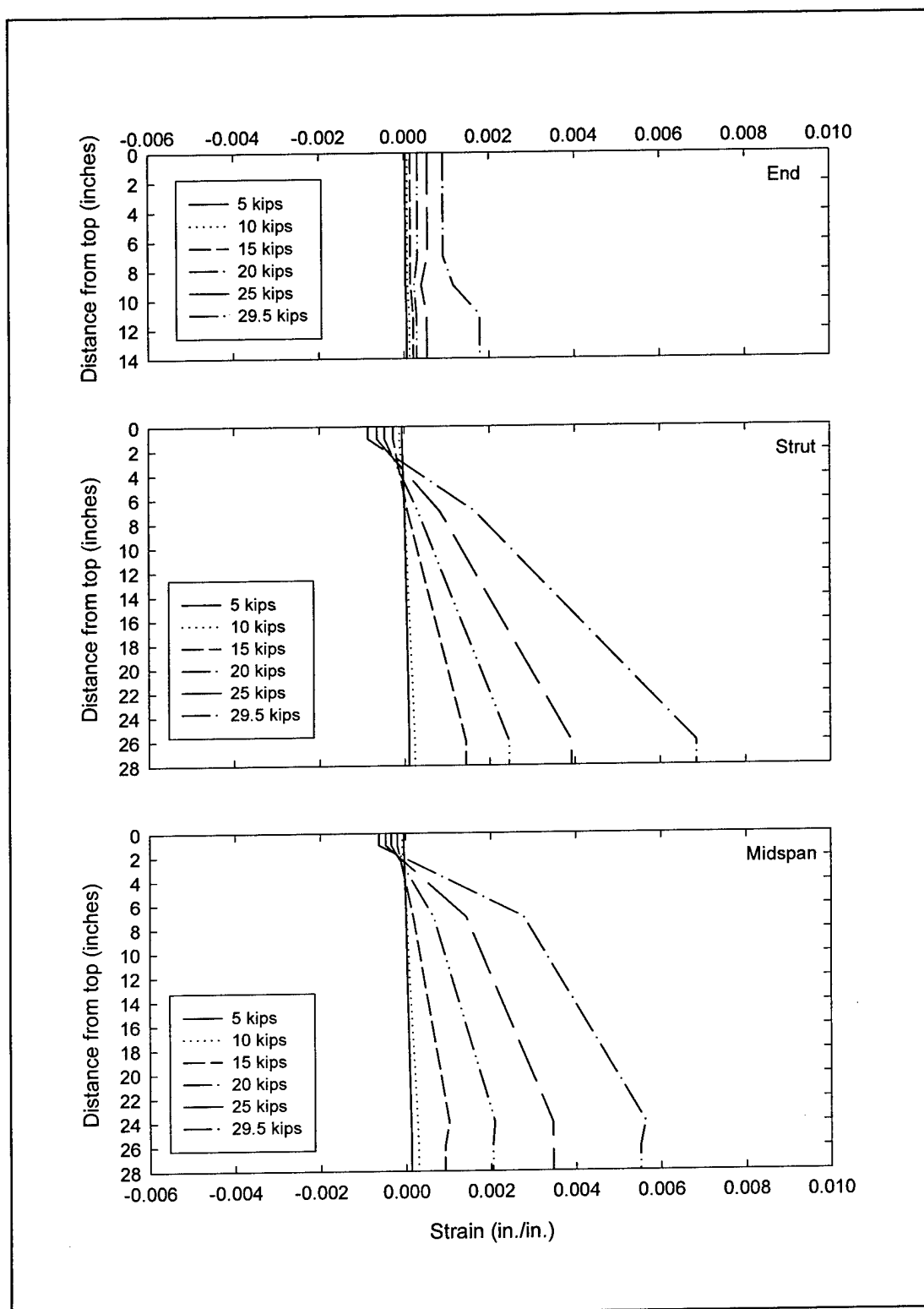
Figure 28. Strain distribution for HJ-7.
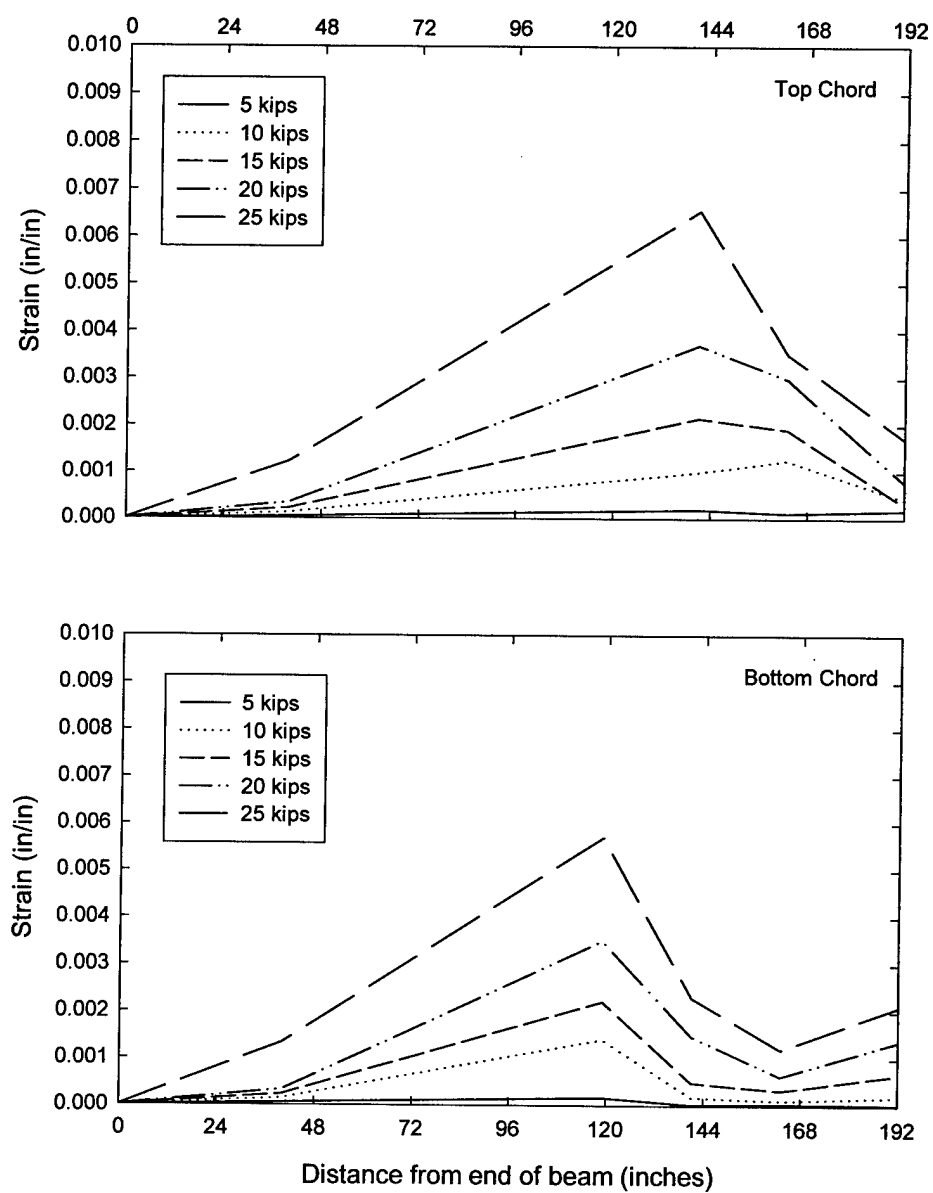
Figure 29. Strain distribution along strand length of HJ-3.
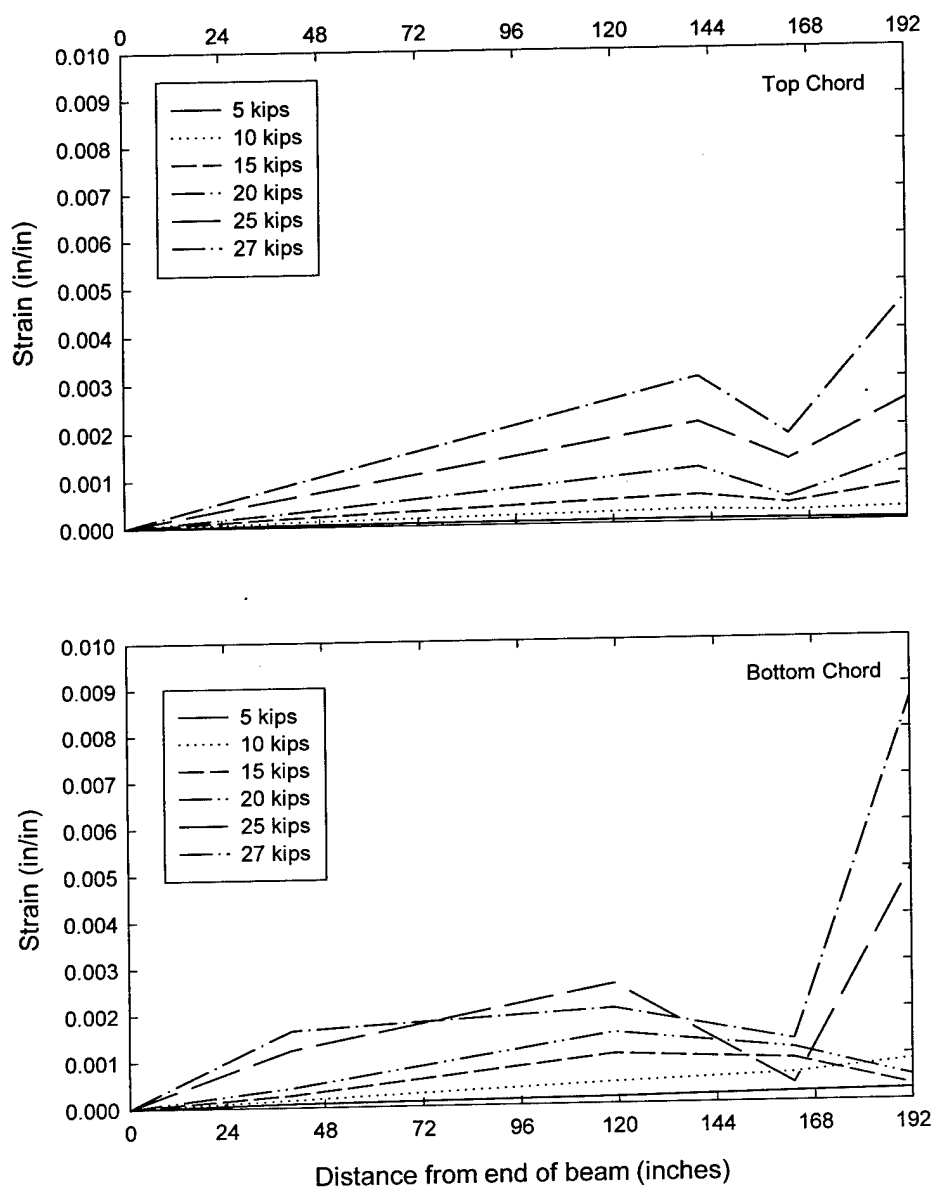
Figure 30. Strain distribution along strand length of HJ-4.
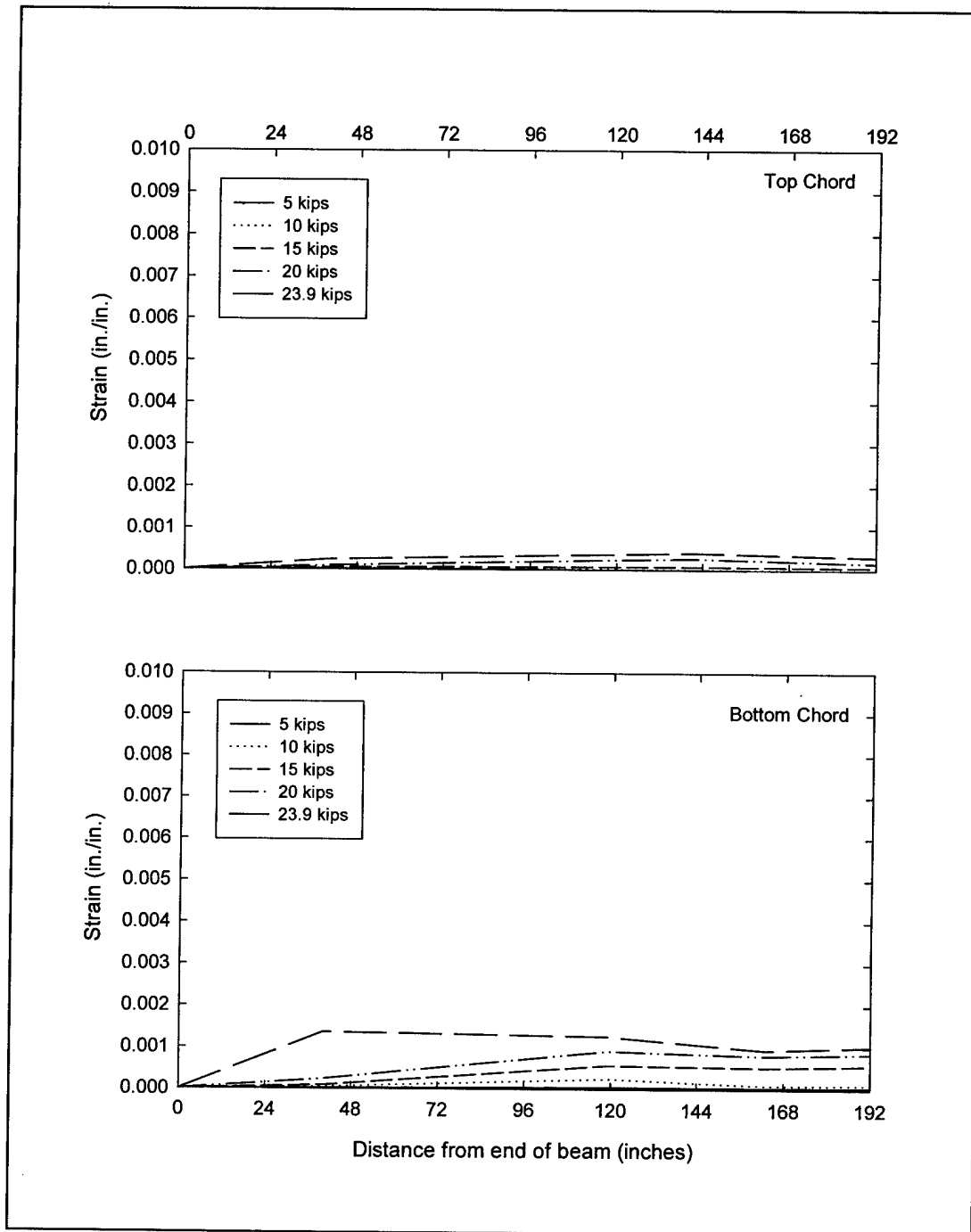
Figure 31. Strain distribution along strand length of HJ-6.
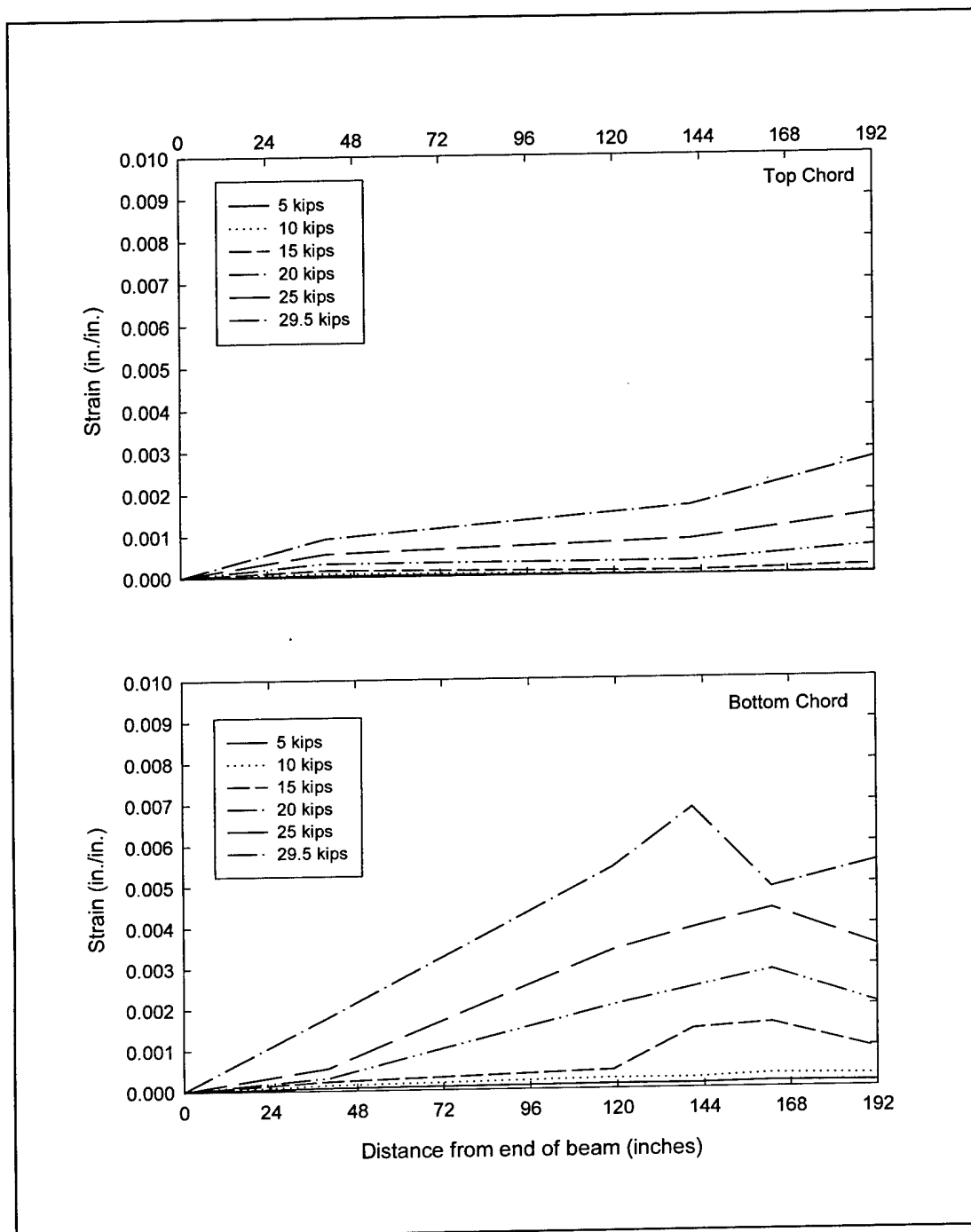
Figure 32. Strain distribution along strand length of HJ-7.
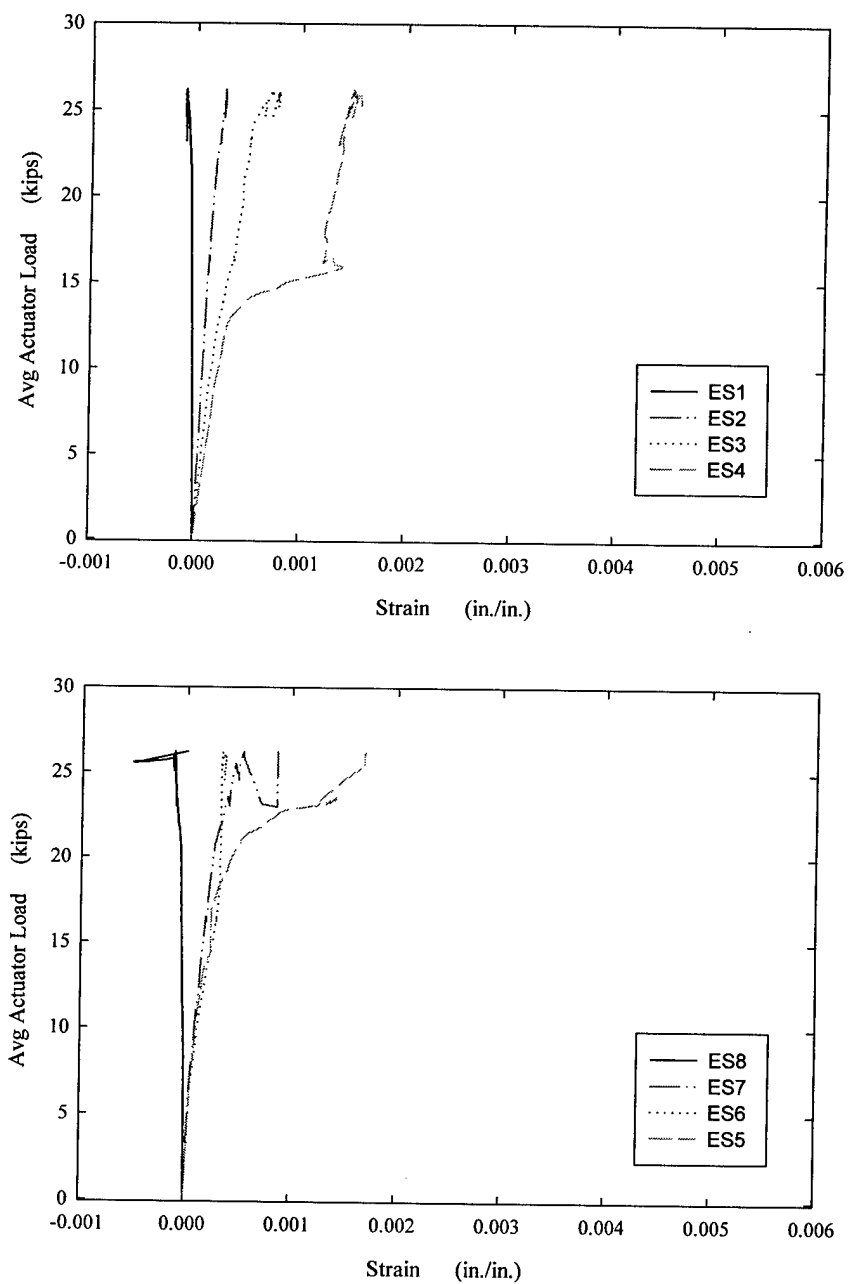
Figure 33. HJ-3 upgrade FRP strains.
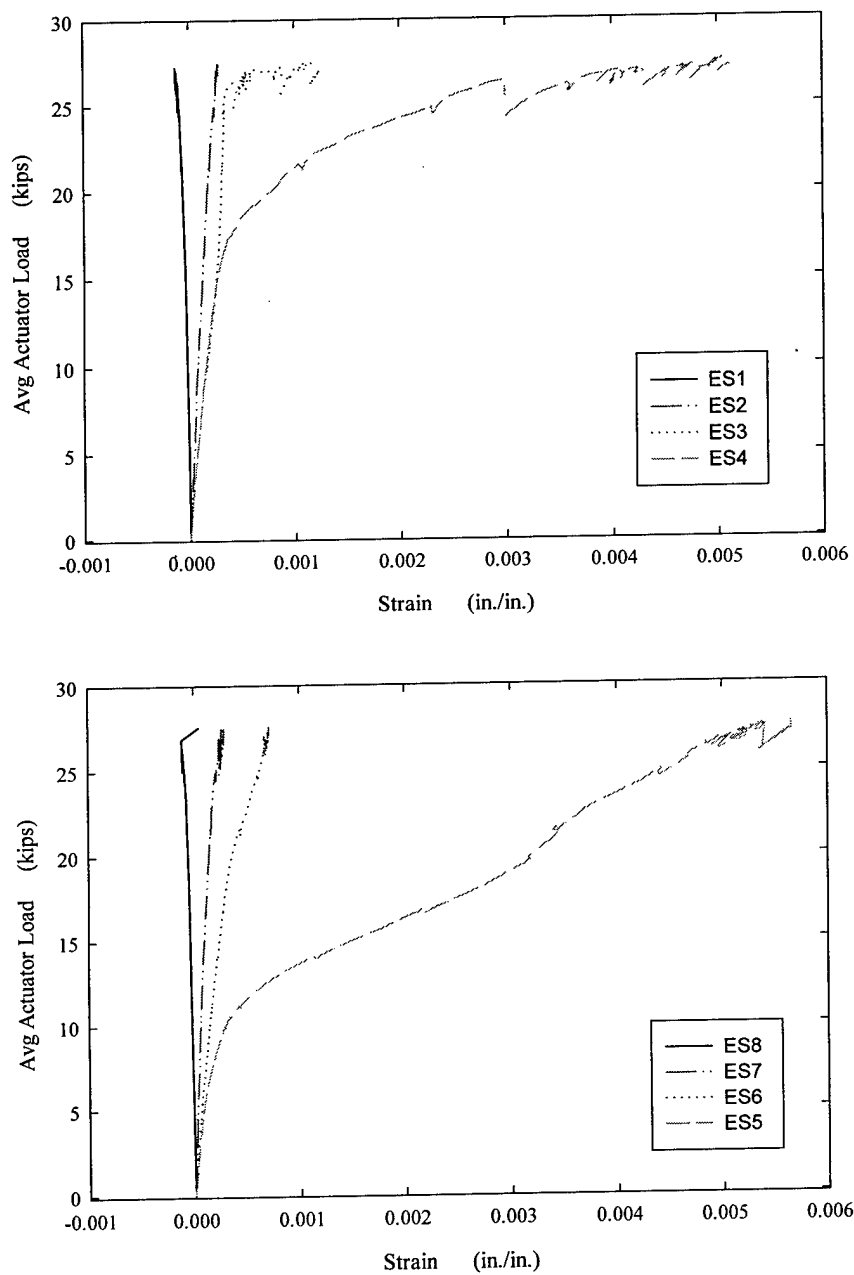
Figure 34. HJ-4 repair FRP strains.

Figure 35. Crack patterns for HJ-6.

Figure 36. Failure of HJ-6.
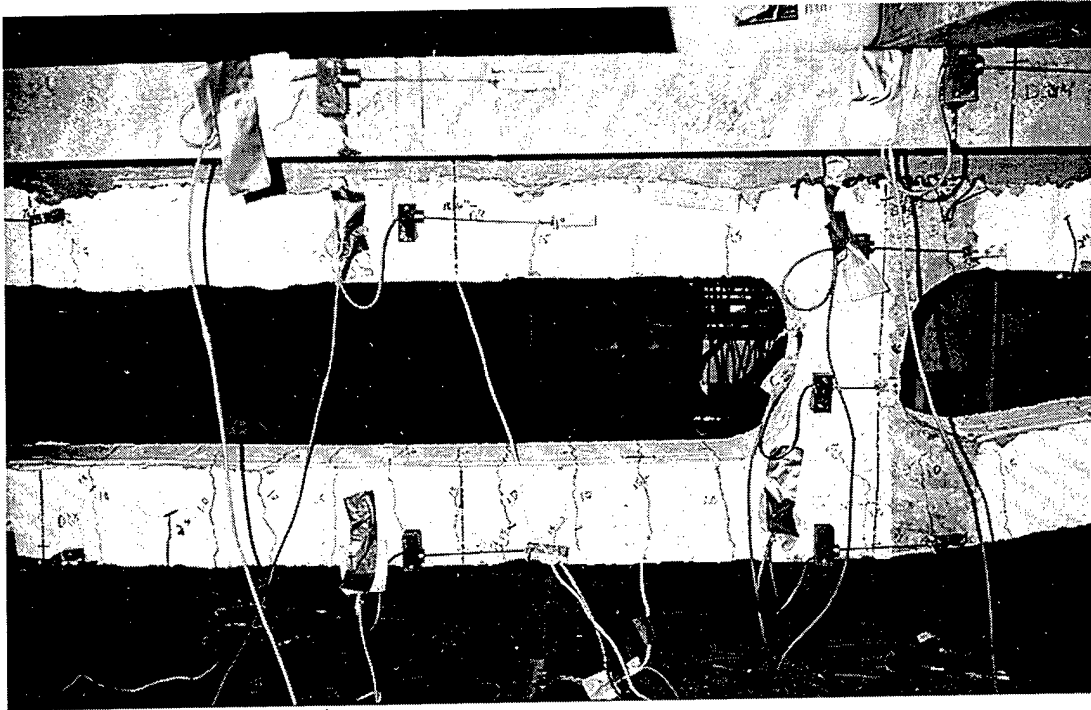
Figure 37. Crack patterns for HJ-7.
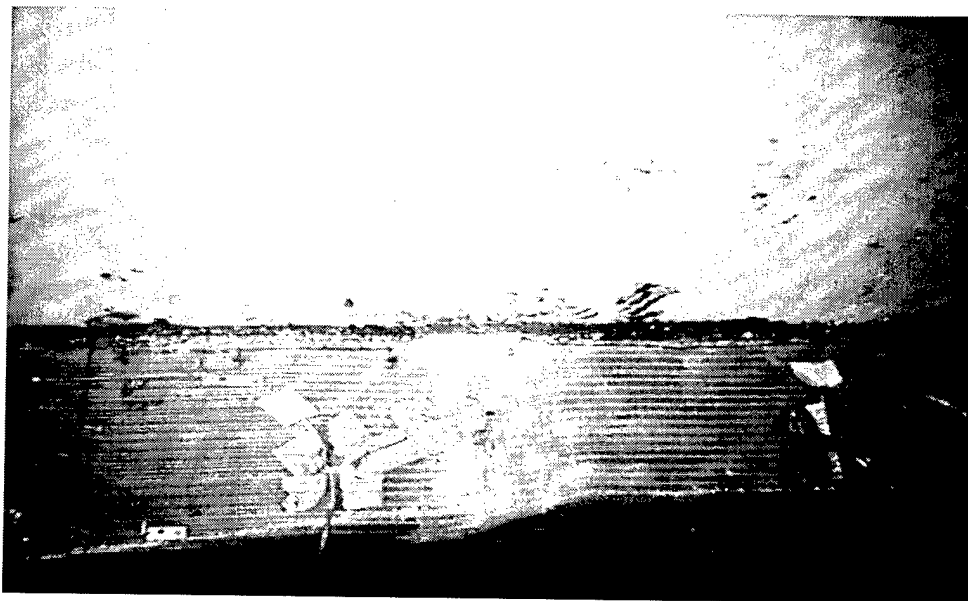
a. Cracks at slab/web interface and in slab at north end of HJ-3.
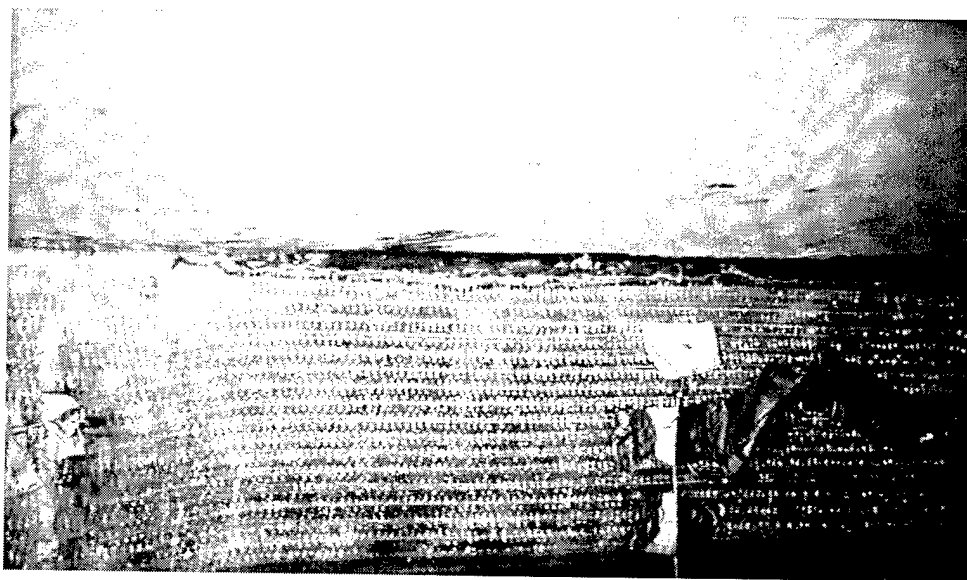
b. Detail of crack at frp edge at slab/web interface of HJ-3.

Figure 38. Crack patterns for HJ-3.
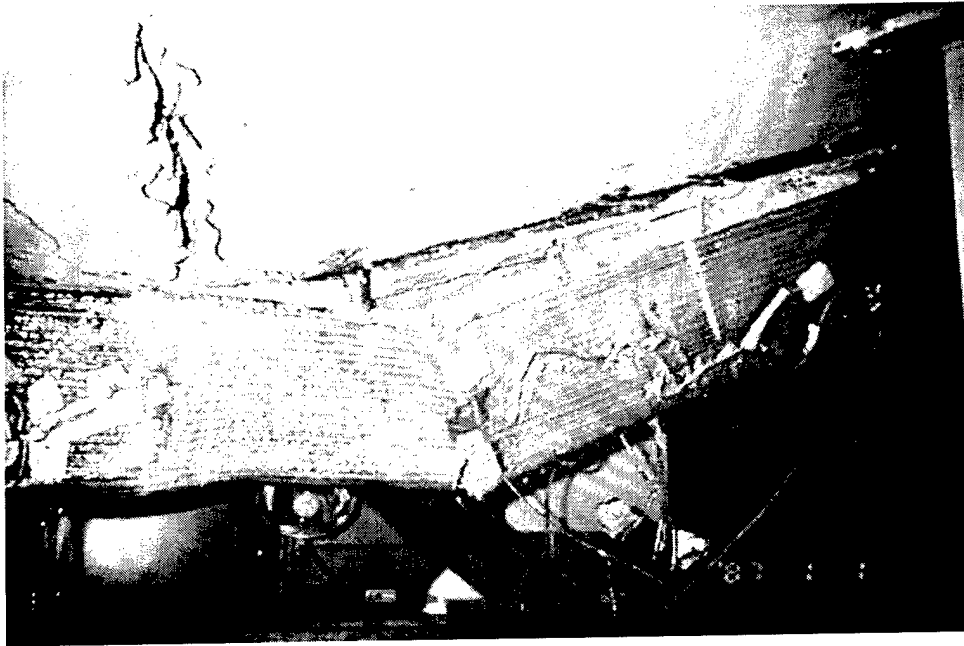
a. Failure at north end of HJ-3
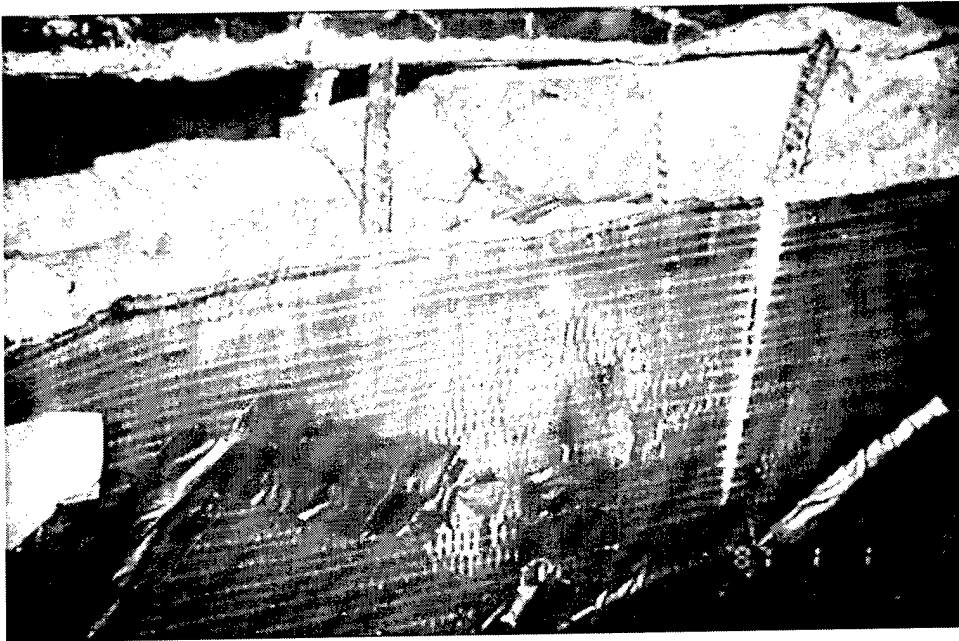
b. Detail of crack and separation at slab/web interface at failure of HJ-3.

Figure 39. Failure of HJ-3.
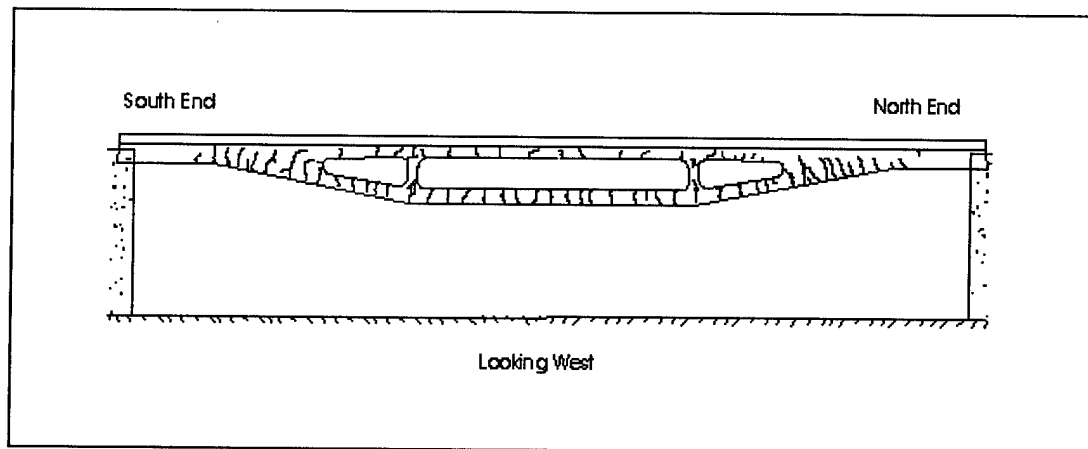
Figure 40. Crack Patterns of HJ-4 prior to FRP repair.
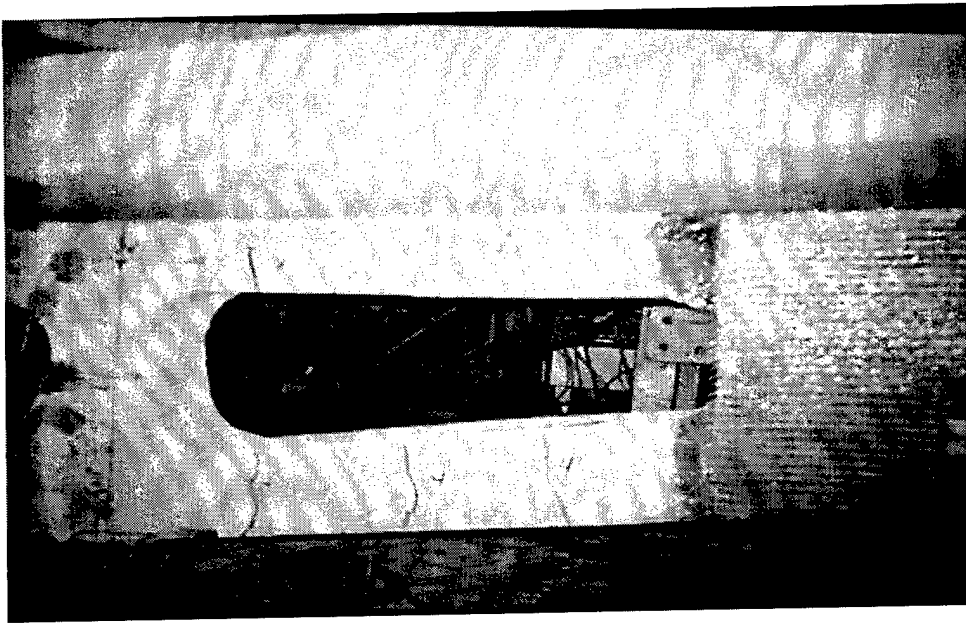
a. Cracks at north end of joist
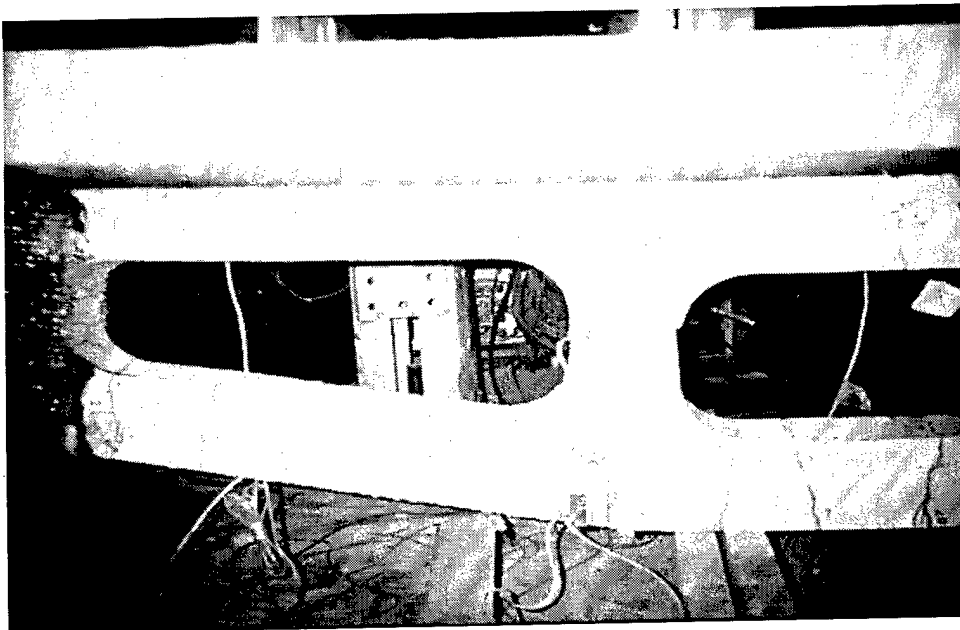
b. Cracks at south end of joist

Figure 41. Crack patterns for HJ-4.

Design Procedure for Shear Repair for Reinforced Concrete Beam using FRP

```
┌─────────────────────────────────────────┐
│ Calculate applied service and ultimate loads │
└─────────────────────────────────────────┘
                    │
┌─────────────────────────────────────────────┐
│    Calculate capacity of existing section     │
│ (based on the provided preliminary design table) │
└─────────────────────────────────────────────┘
                    │
┌──────────────────────────────────┐
│   Calculate the internal forces due to │
│   each case of loading using a frame   │
│         analysis program          │
└──────────────────────────────────┘
                    │
      ⟨ Check ultimate flexural strength ⟩  No → │ change the section │
                    │ OK
           ⟨ allowable initial ⟩  No →
           ⟨ stress at release ⟩
                    │ OK
           ⟨ allowable final ⟩  No →
           ⟨ stress at service ⟩
                    │ OK
      ⟨ Check crack width limit ⟩  No →
                    │ OK
           ⟨ Check deflection ⟩  No → │ increase the concrete │
                    │ OK          │ strength or change the │
                                   │ section               │
  No ⟨ Check vertical shear ⟩
│ use shear reinforcement │      │ OK
                           │ End │
```

Figure 42. Shear repair design procedure.

$w_u = 4 \text{ k/ft}$

25 feet

18 in

12 in
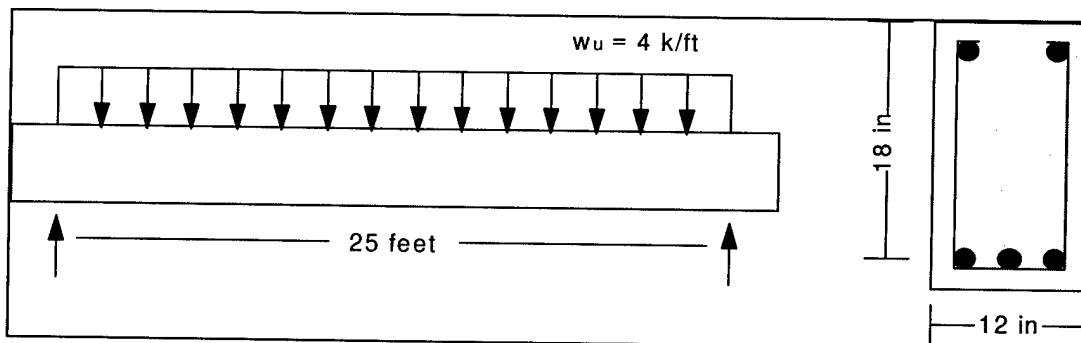
Figure 43. Simply supported beam.
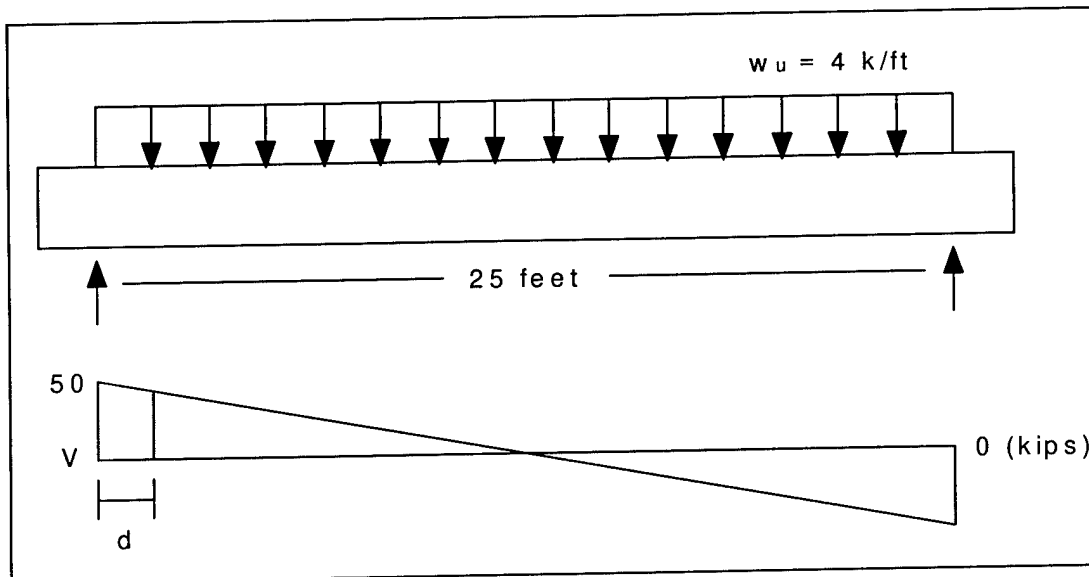
Figure 44. Shear diagram.
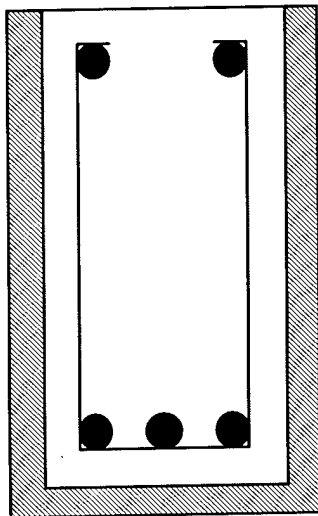
Figure 45. FRP wrap repair.

Table 1. Hybrid Joists Tested

Joist Designation	Configuration	Web Shear Reinforcement	Slab Width (ft)
HJ-3	Upgraded with FRP	Figure 4.6	6
HJ-4	Tested, then repaired with FRP	Figure 4.6	6
HJ-6	Insufficient shear reinforcement	Figure 4.8	4
HJ-7	Proper shear reinforcement	Figure 4.8	4

Table 2. Epoxy Material Properties

Property	Average	Minimum	Test Method
-Tg @ 45% RH	120°F	100°F	
-Tg @ 95% RH	110°F	95°F	
-Tg 140OF Postcure (24 Hours)	180°F	140°F	
Tensile Strength	10,100 psi	9,500 psi	ASTM D 638 Type 1
Tensile Modulus	461,000 psi	425000 psi	ASTM D 638 Type 1
Elongation Percent	5.00%	3.50%	ASTM D 638 Type 1
Flexural Strength	11,500 psi	10,500 psi	ASTM D.790
Flexural Modulus	400,000 psi	375,000 psi	ASTM D 790

Curing Schedule 72 hours post cure at 140°F

Table 3. Yarn Properties

Property	E-glass	Polyaramid	Test Method
Yield/Denier	1200 and 250 ypp	2160 denier	
Density (g/cc)	2.54	1.44	ASTM D 792
Tensile Strength (psi)	440,000	400,000	SIM 13*
Tensile Modulus (psi)	10,500,000	17,000,000	STM 13
Elongation (%)	4.2	2.5	STM 13

* Seguin Test Method - Hexel Manufacturing facility standard methods based on appropriate Standardized testing procedure

Table 4. Fabric Properties

Property	Average Value	Minimum Value	Test Method
Areal Weight (oz/sq. yd.)	27.2	24.4	STM 18
Tensile Strength dry 1" strip (Break Load lb.)	1800	1600	STM 27
Air Permeability (cu. ft./min.)	22	20	STM 26

Table 5. Composite Laminate Specification

Property	Value	ASTM Method
Ultimate Tensile Strength min. (primary fiber direction)*	65,000 psi	D 3039
Elongation at break, min.	2.00%	D 3039
Tensile Modulus	3.0×10^6 psi	
Ultimate Tensile Strength min. (90 degrees to primary fiber direction)	4,800 psi	D 3039

* Tensile retained 7 days @ 100% RH, 1,000 hours ozone, 1,000 hours alkali, 1,000 hours salt water, and 1,000 hours at 140°F
Cured for 48 hours at 140°F Using Hexcel Sample Preparation

Table 6. Composite Material Properties

Property	Value	Test Method
Tensile Strength at 0° (ksi)	65	ASTM D3039
Tensile Strength at 90° (ksi)	6.0	ASTM D3039
Elastic Modulus (ksi)	3,250	
Ultimate Strain	0.02	ASTM D3039
Coefficient of Thermal Expansion	4.3×10^{-6}	

Table 7. Casting and Release Dates for Each Hybrid Joist Web

Specimen	Casting Date	Release Date
HJ-3	1/29/96	2/5/96
HJ-4	1/29/96	2/5/96
HJ-6	2/12/96	2/16/96
HJ-7	6/20/96	6/24/96

Table 8. Instrumentation for HJ-3 Upgraded With FRP

Hybrid Joist Test				HJ-3		Date:	August 12, 1996
USA Construction Engineering Research Laboratories						Champaign, IL	

Instrument	CERL Name/ Cable #	CIR Name	Conversion Factor (per volt)	Location (X - Dir.) (in.)	Location (Y - Dir.) (in.)	Gage Length (in.)	Comments
Cell_N		N / A	5.000 kips	141.000	N / A	N / A	Concentrated Load - 50 Kip Actuator
Stroke_N		N / A	0.300 inches	141.000	N / A	N / A	
Cell_S		N / A	5.000 kips	250.000	N / A	N / A	Concentrated Load - 50 Kip Actuator
Stroke_S		N / A	0.300 inches	250.000	N / A	N / A	
POT_N	P1	N / A	1.994 inches	141.000	N / A	N / A	Third span Deflection - Potentiometer
POT_Mid	P2	N / A	1.996 inches	192.000	N / A	N / A	Midspan Deflection - Potentiometer
POT_S	P3	N / A	2.000 inches	278.000	N / A	N / A	Quarter span Deflection - Potentiometer
Int_1	IS1 / 3	s19	0.00150 in/in	40.000	N / A	N / A	Placed by the CIR
Int_2	IS2 / 2	s20	0.00150 in/in	40.000	N / A	N / A	Placed by the CIR
Int_3	IS3 / 1	s21	0.00150 in/in	40.000	N / A	N / A	Placed by the CIR
Int_4	IS4 / 12	s28	0.00150 in/in	141.000	N / A	N / A	Placed by the CIR
Int_5	IS5 / 11	s26	0.00150 in/in	119.000	N / A	N / A	Placed by the CIR
Int_6	IS6 / 10	s30	0.00150 in/in	141.000	N / A	N / A	Placed by the CIR
Int_7	IS7 / 15	s31	0.00150 in/in	163.000	N / A	N / A	Placed by the CIR
Int_8	IS8 / 14	s27	0.00150 in/in	119.000	N / A	N / A	Placed by the CIR
Int_9	IS9 / 13	s33	0.00150 in/in	163.000	N / A	N / A	Placed by the CIR
Int_10	IS10 / 18	s34	0.00150 in/in	192.000	N / A	N / A	Placed by the CIR
Int_11	IS11 / 17	s35	0.00150 in/in	192.000	N / A	N / A	Placed by the CIR
Int_12	IS12 / 16	s36	0.00150 in/in	192.000	N / A	N / A	Placed by the CIR
LVDT_1	D1	N / A	0.00500 in.	75.500	1.000	7.205	Measured from the Top of the Slab
LVDT_2	D2	N / A	0.00500 in.	74.000	3.000	6.417	Measured from the Bottom Face of the Slab
LVDT_3	D3	N / A	0.00500 in.	73.000	12.250	4.134	Measured from the Bottom Face of the Slab
LVDT_4	D4	N / A	0.00500 in.	145.000	1.000	6.220	Measured from the Top of the Slab
LVDT_5	D5	N / A	0.00500 in.	143.000	3.500	7.480	Measured from the Bottom Face of the Slab
LVDT_6	D6	N / A	0.00500 in.	142.500	11.000	2.677	Measured from the Bottom Face of the Slab
LVDT_7	D7	N / A	0.00500 in.	142.000	22.750	2.756	Measured from the Bottom Face of the Slab
LVDT_8	D8	N / A	0.00500 in.	170.500	1.000	7.520	Measured from the Top of the Slab
LVDT_9	D9	N / A	0.00500 in.	N / A	N / A	N / A	Not used for this test, Sensor moved to D7
LVDT_10	D10	N / A	0.00500 in.	169.250	22.750	5.630	Measured from the Bottom Face of the Slab
LVDT_11	D11	N / A	0.00500 in.	193.500	1.000	5.276	Measured from the Top of the Slab
LVDT_12	D12	N / A	0.00500 in.	194.000	3.000	5.433	Measured from the Bottom Face of the Slab
LVDT_13	D13	N / A	0.00500 in.	194.000	22.500	5.039	Measured from the Bottom Face of the Slab
LVDT_14	D14	N / A	0.00500 in.	193.500	N / A	5.197	Placed on top of Slab
LVDT_15	D15	N / A	0.00500 in.	243.000	N / A	2.677	Not used for this test
LVDT_16	D16	N / A	0.00500 in.	194.000	N / A	6.850	Placed on bottom side of Web
LVDT_17	D17	N / A	- 0.00500 in.	222.000	2.250	2.677	Measured from the Bottom Face of the Slab
LVDT_18	D18	N / A	0.00500 in.	222.000	22.500	4.803	Measured from the Bottom Face of the Slab
LVDT_19	D19	N / A	- 0.00500 in.	242.000	10.000	3.268	Measured from the Bottom Face of the Slab
LVDT_20	D20	N / A	0.00500 in.	242.000	22.000	2.480	Measured from the Bottom Face of the Slab

Instrument	CERL Name/ Cable #	CIR Name	Conversion Factor (per volt)	Location (X - Dir.) (in.)	Location (Y - Dir.) (in.)	Gage Length (in.)	Comments
Hybrid Joist Test			HJ-3	Date:	August 12, 1996		
USA Construction Engineering Research Laboratories					Champaign, IL		
Ext. Str._1	ES1	N / A	0.00150 in/in				
Ext. Str._2	ES2	N / A	0.00150 in/in				
Ext. Str._3	ES3	N / A	0.00150 in/in	See Attached Figure for External			
Ext. Str._4	ES4	N / A	0.00150 in/in	Strain Gage Locations			
Ext. Str._5	ES5	N / A	0.00150 in/in				
Ext. Str._6	ES6	N / A	0.00150 in/in				
Ext. Str._7	ES7	N / A	0.00150 in/in				
Ext. Str._8	ES8	N / A	0.00150 in/in				

*** +X direction is defined as running north to south with north being 0. Measurements taken to the north face of the LVDT blocks.

*** +Y direction is defined as running up to down with 0 being the bottom face of the slab, except where noted that measurement was taken from the top of the slab. Measurement was taken to the middle of the circular opening in the block.

IMPORTANT NOTE: Sensor for D7 was not working. Sensor from D9 was placed in location of D7.

Table 9. Instrumentation for HJ-4 Without FRP Repair

Hybrid Joist Test		HJ-4		Date: June 3, 1996			
USA Construction Engineering Research Laboratories						(First Test without FRP)	
Instrument	CERL Name/ Cable #	CIR Name	Conversion Factor (per volt)	Location (X - Dir.) (in.)	Location (Y - Dir.) (in.)	Gage Length (in.)	Comments
Cell_N		N / A	5.000 kips	141.000	N / A	N / A	Concentrated Load - 50 Kip Actuator
Stroke_N		N / A	0.300 inches	141.000	N / A	N / A	
Cell_S		N / A	5.000 kips	250.000	N / A	N / A	Concentrated Load - 50 Kip Actuator
Stroke_S		N / A	0.300 inches	250.000	N / A	N / A	
POT_N	P1	N / A	1.994 inches	141.000	N / A	N / A	Third span Deflection - Potentiometer
POT_Mid	P2	N / A	1.996 inches	192.000	N / A	N / A	Midspan Deflection - Potentiometer
POT_S	P3	N / A	2.000 inches	278.000	N / A	N / A	Quarter span Deflection - Potentiometer
Int_1	IS1 / 19	s19	0.00150 in/in	40.000	N / A	N / A	Placed by the CIR
Int_2	IS2 / 16	s20	0.00150 in/in	40.000	N / A	N / A	Placed by the CIR
Int_3	IS3 / 21	s21	0.00150 in/in	40.000	N / A	N / A	Placed by the CIR
Int_4	IS4 / 28	s28	0.00150 in/in	141.000	N / A	N / A	Placed by the CIR
Int_5	IS5 / 26	s26	0.00150 in/in	119.000	N / A	N / A	Placed by the CIR
Int_6	IS6 / 30	s30	0.00150 in/in	141.000	N / A	N / A	Placed by the CIR
Int_7	IS7 / 31	s31	0.00150 in/in	163.000	N / A	N / A	Placed by the CIR
Int_8	IS8 / 27	s27	0.00150 in/in	119.000	N / A	N / A	Placed by the CIR
Int_9	IS9 / 33	s33	0.00150 in/in	163.000	N / A	N / A	Placed by the CIR
Int_10	IS10 / 34	s34	0.00150 in/in	192.000	N / A	N / A	Placed by the CIR
Int_11	IS11 / 35	s35	0.00150 in/in	192.000	N / A	N / A	Placed by the CIR
Int_12	IS12 / 36	s36	0.00150 in/in	192.000	N / A	N / A	Placed by the CIR
LVDT_1	D1	N / A	0.00494 in.	72.750	1.000	7.205	Measured from the Top of the Slab
LVDT_2	D2	N / A	0.00497 in.	71.375	3.000	6.063	Measured from the Bottom Face of the Slab
LVDT_3	D3	N / A	0.00495 in.	69.125	12.250	2.913	Measured from the Bottom Face of the Slab
LVDT_4	D4	N / A	0.00497 in.	145.125	1.000	5.748	Measured from the Top of the Slab
LVDT_5	D5	N / A	0.00496 in.	143.375	3.500	5.197	Measured from the Bottom Face of the Slab
LVDT_6	D6	N / A	0.00496 in.	143.375	11.000	2.559	Measured from the Bottom Face of the Slab
LVDT_7	D7	N / A	0.00496 in.	142.375	22.750	5.236	Measured from the Bottom Face of the Slab
LVDT_8	D8	N / A	0.00495 in.	168.125	1.000	5.236	Measured from the Top of the Slab
LVDT_9	D9	N / A	0.00496 in.	167.375	3.000	2.441	Measured from the Bottom Face of the Slab
LVDT_10	D10	N / A	0.00499 in.	168.375	22.750	2.441	Measured from the Bottom Face of the Slab
LVDT_11	D11	N / A	0.00489 in.	195.000	1.000	6.417	Measured from the Top of the Slab
LVDT_12	D12	N / A	0.00496 in.	193.875	3.000	7.283	Measured from the Bottom Face of the Slab
LVDT_13	D13	N / A	0.00496 in.	195.500	22.500	5.197	Measured from the Bottom Face of the Slab

Instrument	CERL Name/ Cable #	CIR Name	Conversion Factor (per volt)	Location (X - Dir.) (in.)	Location (Y - Dir.) (in.)	Gage Length (in.)	Comments
Hybrid Joist Test			HJ-4		Date: June 3, 1996		
USA Construction Engineering Research Laboratories						(First Test without FRP)	
LVDT_14	D14	N / A	0.00491 in.	194.750	N / A	6.260	Placed on top of Slab
LVDT_15	D15	N / A	0.00496 in.	N / A	N / A	N / A	Not used for this test, Sensor moved to D13
LVDT_16	D16	N / A	0.00500 in.	195.250	N / A	6.299	Placed on bottom side of Web
LVDT_17	D17	N / A	-0.00503 in.	220.000	2.250	7.638	Measured from the Bottom Face of the Slab
LVDT_18	D18	N / A	0.00487 inches	220.375	22.500	4.055	Measured from the Bottom Face of the Slab
LVDT_19	D19	N / A	-0.00501 in.	244.000	10.000	2.362	Measured from the Bottom Face of the Slab
LVDT_20	D20	N / A	0.00500 in.	244.125	22.000	2.717	Measured from the Bottom Face of the Slab

*** +X direction is defined as running north to south with north being 0. Measurements taken to the north face of the LVDT blocks.

*** +Y direction is defined as running up to down with 0 being the bottom face of the slab, except where noted that measurement was taken from the top of the slab. Measurement was taken to the middle of the circular opening in the block.

IMPORTANT NOTES: Sensor for D15 was moved into the D13 position. D15 position was not used.

Table 10. Instrumentation for HJ-4 With FRP Repair

Hybrid Joist Test   HJ-4   (2nd Test with FRP)
USA Construction Engineering Research
Laboratories
Champaign, IL

Date: August 2
             1996

Instrument	CERL Name / Cable #	CIR Name	Conversion Factor (per volt)	Location (X - Dir.) (in.)	Location (Y - Dir.) (in.)	Gage Length (in.)	Comments
Cell_N		N / A	5.000 kips	141.000	N / A	N / A	Concentrated Load - 50 Kip Actuator
Stroke_N		N / A	0.300 inches	141.000	N / A	N / A	
Cell_S		N / A	5.000 kips	250.000	N / A	N / A	Concentrated Load - 50 Kip Actuator
Stroke_S		N / A	0.300 inches	250.000	N / A	N / A	
POT_N	P1	N / A	2.000 inches	141.000	N / A	N / A	Third span Deflection - Potentiometer
POT_Mid	P2	N / A	2.000 inches	192.000	N / A	N / A	Midspan Deflection - Potentiometer
POT_S	P3	N / A	2.000 inches	278.000	N / A	N / A	Quarter span Deflection - Potentiometer
Int_1	IS1 / 19	s19	0.00150 in/in	40.000	N / A	N / A	Placed by the CIR
Int_2	IS2 / 16	s20	0.00150 in/in	40.000	N / A	N / A	Placed by the CIR
Int_3	IS3 / 21	s21	0.00150 in/in	40.000	N / A	N / A	Placed by the CIR
Int_4	IS4 / 28	s28	0.00150 in/in	141.000	N / A	N / A	Placed by the CIR
Int_5	IS5 / 26	s26	0.00150 in/in	119.000	N / A	N / A	Placed by the CIR
Int_6	IS6 / 30	s30	0.00150 in/in	141.000	N / A	N / A	Placed by the CIR
Int_7	IS7 / 31	s31	0.00150 in/in	163.000	N / A	N / A	Placed by the CIR
Int_8	IS8 / 27	s27	0.00150 in/in	119.000	N / A	N / A	Placed by the CIR
Int_9	IS9 / 33	s33	0.00150 in/in	163.000	N / A	N / A	Placed by the CIR
Int_10	IS10 / 34	s34	0.00150 in/in	192.000	N / A	N / A	Placed by the CIR
Int_11	IS11 / 35	s35	0.00150 in/in	192.000	N / A	N / A	Placed by the CIR
Int_12	IS12 / 36	s36	0.00150 in/in	192.000	N / A	N / A	Placed by the CIR
LVDT_1	D1	N / A	0.00500 inches	72.750	1.000	7.205	Measured from the Top of the Slab
LVDT_2	D2	N / A	0.00500 inches	69.000	3.000	6.000	Measured from the Bottom Face of the Slab
LVDT_3	D3	N / A	0.00500 inches	68.500	12.000	3.125	Measured from the Bottom Face of the Slab
LVDT_4	D4	N / A	0.00500 inches	145.125	1.000	5.748	Measured from the Top of the Slab
LVDT_5	D5	N / A	0.00500 inches	143.375	3.500	5.197	Measured from the Bottom Face of the Slab
LVDT_6	D6	N / A	0.00500	143.375	11.000	2.559	Measured from the Bottom

Hybrid Joist Test   HJ-4   (2nd Test with FRP)

USA Construction Engineering Research
Laboratories
Champaign, IL

Date: August 2
             1996

Instrument	CERL Name / Cable #	CIR Name	Conversion Factor (per volt)	Location (X - Dir.) (in.)	Location (Y - Dir.) (in.)	Gage Length (in.)	Comments
LVDT_7	D7	N / A	inches 0.00500	142.375	22.750	5.236	Face of the Slab Measured from the Bottom Face of the Slab
LVDT_8	D8	N / A	inches 0.00500	168.125	1.000	5.236	Measured from the Top of the Slab
LVDT_9	D9	N / A	inches N / A	N / A	N / A	N / A	Not used for this test, Sensor moved to D5
LVDT_10	D10	N / A	0.00500 inches	168.375	22.750	2.441	Measured from the Bottom Face of the Slab
LVDT_11	D11	N / A	0.00500 inches	195.000	1.000	6.417	Measured from the Top of the Slab
LVDT_12	D12	N / A	0.00500 inches	193.875	3.000	7.283	Measured from the Bottom Face of the Slab
LVDT_13	D13	N / A	0.00500 inches	195.500	22.500	5.197	Measured from the Bottom Face of the Slab
LVDT_14	D14	N / A	0.00500 inches	194.750	N / A	6.260	Placed on top of Slab
LVDT_15	D15	N / A	N / A	N / A	N / A	N / A	Not used for this test, Sensor moved to D13
LVDT_16	D16	N / A	0.00500 inches	195.250	N / A	6.299	Placed on bottom side of Web
LVDT_17	D17	N / A	- 0.00500 in.	220.000	2.250	7.638	Measured from the Bottom Face of the Slab
LVDT_18	D18	N / A	0.00500 inches	220.375	22.500	4.055	Measured from the Bottom Face of the Slab
LVDT_19	D19	N / A	- 0.00500 in.	244.000	10.000	2.362	Measured from the Bottom Face of the Slab
LVDT_20	D20	N / A	0.00500 inches	244.125	22.000	2.717	Measured from the Bottom Face of the Slab
Ext. Str._1	ES1	N / A	0.00150 in / in				
Ext. Str._2	ES2	N / A	0.00150 in / in				
Ext. Str._3	ES3	N / A	0.00150 in / in			See Attached Figure for Externa Strain Gage Locations	
Ext. Str._4	ES4	N / A	0.00150 in / in				
Ext. Str._5	ES5	N / A	0.00150 in / in				
Ext. Str._6	ES6	N / A	0.00150 in / in				
Ext. Str._7	ES7	N / A	0.00150 in / in				

Hybrid Joist Test HJ-4 (2nd Test with FRP)
USA Construction Engineering Research
Laboratories
Champaign, IL

Date: August 2
1996

Instrument	CERL Name / Cable #	CIR Name	Conversion Factor (per volt)	Location (X - Dir.) (in.)	Location (Y - Dir.) (in.)	Gage Length (in.)	Comments
Ext. Str._8	ES8	N / A	0.00150 in / in				

*** +X direction is defined as running north to south with north being 0. Measurements taken to the north face of the LVDT blocks.

*** +Y direction is defined as running up to down with 0 being the bottom face of the slab, except where noted that measurement was taken from the top of the slab. Measurement was taken to the middle of the circular opening in the block.

IMPORTANT NOTES:

Sensor for D15 was moved into the D13 position. D15 position was not used.

Sensor for D9 was moved into the D5 position. D9 position was not used.

Table 11. Principal Experimental Test Results for Hybrid Joists

Joist designation	Experimental cracking load* (kips)	First Crack Location	Applied Failure load* (kips)	Total Failure Load (kips)	Equivalent Uniform Load (ksf)	Type of failure
HJ-3		midspan, bottom chord	52.0	53.0	0.62	shear
HJ-4		midspan, bottom chord	56.6	56.6**	0.67	no failure
HJ-6	11.7	midspan, bottom chord	48.0	49.0	0.57	shear
HJ-7	31.5	midspan bottom chord	64.0	65.0	0.76	flexure

* Sum of two actuators.
**No failure occurred.

Table 12. Camber and Deflection for Hybrid Joists (in.)

Joist designation	Camber at release	LL Deflection	SIDL + LL Deflection	Deflection at peak load	Deflection at failure
HJ-3	0.40	.09	.14	5.66	12.58
HJ-4 without FRP	0.45	.10	.16	7.66	7.67*
HJ-4 with FRP repair	NA	.10	.16	8.62	10.06*
HJ-6	0.45	0.03	0.16	3.52	3.52
HJ-7	0.38	0.02	0.14	16.6	16.6

* Deflection at end of test; no failure occurred.

CERL DISTRIBUTION

Chief of Engineers
    ATTN: CEHEC-IM-LH (2)
    ATTN: CEHEC-IM-LP (2)
    ATTN: CECW
    ATTN: CECW-O
    ATTN: CECW-P
    ATTN: CECW-PR
    ATTN: CEMP-CE
    ATTN: CERD-L

ACS(IM) 22060
    ATTN: DAIM-FDP

CEISC 22310-3862
    ATTN: CEISC-E
    ATTN: CEISC-FT
    ATTN: CEISC-ZC

US Army Engr District
    ATTN: Library (40)

US Army Engr Division
    ATTN: Library (8)

US Army Engineering and Support Center
    ATTN: CEHND 35807-4301

Naval Facilities Engr Command
    ATTN: Facilities Engr Command (8)
    ATTN: Engrg Field Divisions (10)
    ATTN: Engrg Field Activities (4)
    ATTN: Public Works Center (8)
    ATTN: Naval Constr Battalion Ctr 93043
    ATTN: Naval Facil Engr Service Ctr 93043-4328

Tyndall AFB 32403
    ATTN: HQAFCESA/CES
    ATTN: Engrg & Srvc Lab

American Public Works Assoc. 64104-1806

US Gov't Printing Office 20401
    ATTN: Rec Sec/Deposit Sec (2)

Defense Tech Info Center 22060-6218
    ATTN: DTIC-O (2)

                                         103
                                       3/98